J. Fluid Mech. (1996), *vol.* 329, *pp.* 413–443

A uniformly asymptotic approximation for the development of shear dispersion

By C. G. PHILLIPS[1,2] AND S. R. KAYE[1]

[1]Physiological Flow Studies Group, Centre for Biological and Medical Systems and
[2]Department of Mathematics, Imperial College of Science, Technology and Medicine,
Prince Consort Road, London SW7 2BY, UK

(Received 15 February 1996 and in revised form 14 June 1996)

In this paper we consider the development of shear dispersion following the introduction of a diffusing tracer substance into a tube or duct containing flowing fluid, with emphasis on the characterization of the temporal variation of concentration at a fixed axial position. Asymptotic results are derived by assuming that the distance downstream of the point of tracer introduction, appropriately non-dimensionalized, is large. First, we consider the central moments of the temporal concentration variation, including their dependence on transverse position and on the initial transverse distribution of tracer. The moments for finite Péclet number are expressed in terms of their infinite-Péclet-number counterparts, and the latter are given explicitly for Poiseuille flow. Then, assuming the Péclet number is infinite, we derive an approximate solution for the Green's function expressing tracer concentration following its introduction at an arbitrary point within the tube. The solution is expressed in terms of three numerically evaluated functions of a dimensionless time variable, with parametric dependence on the distance downstream of the point of tracer release. The method is illustrated by calculation of the approximate solution for dispersion in Poiseuille flow. Unlike previous approximations, the present solution is uniformly asymptotic and represents the tails of the concentration distribution as well as the approximately Gaussian central part; in these three regions, simpler analytic forms of the approximation are given. Comparison with previous computational solutions suggests the present approximation remains reasonably accurate even at quite short distances from the point where tracer is released.

1. Introduction

The basic phenomenon of dispersion in shear flows has been understood since Taylor (1953, 1954) considered the transport of a diffusing tracer substance following its introduction into Poiseuille flow. He showed that, because of its diffusive migration between different streamlines, the tracer eventually experiences not only translatory motion with the mean flow velocity, but also an apparently diffusive spreading in the axial direction. When the Péclet number P, which expresses the strength of advection relative to diffusion, is large, the effective diffusivity greatly exceeds the molecular diffusivity of the tracer. As a result, at large times, the tracer concentration distribution can be approximated by a Gaussian whose mean translates with the average flow velocity and whose variance increases at a rate determined by this effective diffusivity, or shear dispersion coefficient. In this approximation, the concentration is uniform

over the cross-section of the tube, and depends only on the initial axial position of tracer, not on its initial cross-sectional distribution.

Since the original work of Taylor (and its extension by Aris 1956 to include the additional contribution of molecular diffusivity to axial dispersion) there have been many further studies, with applications ranging from the spreading of pollutants in rivers and estuaries, through chemical engineering processes such as chromatography, to gas transport in the bronchial airways and the dispersion of tracers in blood vessels. The theory has been developed in two main directions. On the one hand, it has been shown that similar shear dispersion occurs in a range of other systems, and the corresponding dispersion coefficients have been evaluated (the examples include turbulent pipe flow, flow in channels, oscillatory flow, flow in pipes or ducts with transfer of heat or mass between phases, or with chemical reactions, or with sedimentation, and flow which is not unidirectional but is spatially periodic). On the other hand, it has been recognized that dispersive transport may take a significant time to become established following the introduction of the tracer substance, since it develops on the timescale required for a molecule to diffuse transversely across the tube. As a result, the Gaussian approximation derived by Taylor may not be adequate at a given location if the tube is short or if the Péclet number is high. Under these conditions, not only is the axial distribution non-Gaussian, but the radial distribution is non-uniform and the concentration depends on the initial radial distribution of tracer as well as its axial position. The form of the developing concentration distribution appropriate at earlier times has been investigated extensively, using a variety of approaches. One of the most common, following Aris (1956), is to calculate the time-evolution of the axial moments of the tracer distribution. For Poiseuille flow, such moments have been calculated in various cases by Chatwin (1970), Gill & Sankarasubramanian (1970, 1971) and Smith (1981*b*, 1982*a*, 1984).

Other investigators have found asymptotic approximations for the spatial concentration distribution rather than calculating the axial moments. Some of these are appropriate at very short times, when the effect of diffusion is to modify slightly the effect of pure advection, so that dispersion is absent and the initial tracer distribution is all-important (e.g. Lighthill 1966; Stokes & Barton 1990). Others are appropriate at large times, and essentially describe small departures from the Gaussian form, including the weak radial dependence of the concentration (Chatwin 1970, later extended by Stokes & Barton 1990). They suffer, however, from not being uniformly asymptotic, in the sense that however large the time is, accuracy is lost at some point in the description of the tails of the axial distribution.

In addition to these asymptotic solutions, there have been many other approximate treatments, some of them semi-empirical, aimed at allowing efficient computational estimation of the concentration distribution (e.g. Gill & Sankarasubramanian (1970, 1971), Smith (1981*a*, 1982*b*, 1987*a*, *b*, 1990, 1995), Young & Jones (1991), Camacho (1993)). In addition, concentration distributions have been calculated by computational solution of the full advection-diffusion equation (e.g. Shankar & Lenhoff 1989, 1991; Stokes & Barton, 1990).

The emphasis in dispersion studies has generally been on characterizing the axial concentration distribution at different times. However, in practical applications, what is often required is knowledge about the variation with time of the concentration at a fixed axial position. Unfortunately, there is no straightforward equivalence between the spatial moments at a fixed time and the temporal moments at a fixed position, which limits the applicability of the traditional approach to the study of developing dispersion. In particular, even in developed dispersion the temporal moments beyond

the mean are not equal to those for a translating, spreading Gaussian, though some attempts have been made to calculate them on this assumption (Levenspiel & Smith 1957; Ultman & Weaver 1979). However, for a general class of problems with infinite P there have been calculations of the temporal mean and variance (Smith 1984, 1985) and, at leading order, of the temporal skewness (Chatwin 1980; Smith, 1984). The first three temporal moments have also been calculated numerically for parabolic flow in a channel by Tsai & Holley (1978, 1980). Of course, analytic approximations for the full concentration distribution, rather than its moments, are applicable to both temporal and spatial measurements; there have also been some computational calculations of the time-varying concentration at a fixed position (Shankar & Lenhoff 1989, 1991).

In this paper we use asymptotic techniques to investigate the development of shear dispersion, with emphasis on the temporal variation of concentration at a fixed position downstream of the point where the tracer is released. Two stages of approximation are involved, both based on the assumption that the appropriately non-dimensionalized downstream distance, z, is large. First, in treating the temporal moments (§3), we neglect contributions which decay exponentially with z. In this approximation, we show how to express the finite-P temporal moments in terms of their infinite-P counterparts (unlike the relationship for axial moments, this is not trivial). For Poiseuille flow and for infinite P, we calculate explicitly the first three central moments of the temporal distribution, including the dependence on transverse position and on the initial transverse distribution of tracer. The second stage (§§4,5) is to neglect, in addition, contributions which are algebraically small when z is large. Assuming once again that P is infinite, we derive a uniformly asymptotic approximation for the Green's function expressing the temporal (and radial) downstream concentration distribution, when tracer is initially concentrated at an arbitrary point in the tube. Results are given for Poiseuille flow, and the behaviour is examined in the central region, where Taylor's approximation applies, and in the tails of the distribution. The accuracy of the approximation is investigated by comparison with numerical solutions (Shankar & Lenhoff, 1991). Finally, in §6, as an illustration we summarize the main steps of the derivation and give examples of the approximate solutions for dispersion in Poiseuille flow in dimensional form.

2. Mathematical formulation

For generality, we consider initially the transport of a tracer substance in a tube or duct of arbitrary uniform cross-section, as a result of advection by a unidirectional (and so axially uniform) but otherwise arbitrary flow field, and diffusion with an isotropic and uniform diffusivity. Denoting dimensional time by T, axial distance by Z, transverse position by $\boldsymbol{R}$ and axial velocity by $V(\boldsymbol{R})$, we define, as usual in dispersion studies, the dimensionless variables

$$t = DT/a^2, \qquad z = Z/Pa, \qquad \boldsymbol{r} = \boldsymbol{R}/a, \qquad v(\boldsymbol{r}) = V(\boldsymbol{R})/V_m, \tag{2.1}$$

where D is the tracer diffusivity, a a representative dimension of the cross-section, V_m the cross-sectionally averaged velocity and P the Péclet number expressing the relative importance of advection and diffusion:

$$P = V_m a/D. \tag{2.2}$$

When the tube is circular it is natural to set the lengthscale a equal to its radius; it will be convenient to extend this definition to the general case by choosing a so that the

cross-sectional area of the tube is πa^2. With this choice, if $\mathscr{M}$ denotes the total mass of tracer present, a suitably non-dimensionalized version of the tracer concentration C is

$$c = \pi V_m a^4 C / \mathscr{M} D. \tag{2.3}$$

In terms of the variables just defined, the dimensionless form of the advection–diffusion equation within the tube is

$$\frac{\partial c}{\partial t} + v(\boldsymbol{r})\frac{\partial c}{\partial z} = \nabla_r^2 c + P^{-2}\frac{\partial^2 c}{\partial z^2}, \tag{2.4}$$

in which ∇_r represents the part of the vector differential operator corresponding to the transverse spatial variable $\boldsymbol{r}$. The walls of the tube are assumed to be impermeable to tracer, so the boundary condition there is

$$\frac{\partial c}{\partial n} = 0 \qquad \text{for} \quad \boldsymbol{r} \in \partial K, \tag{2.5}$$

in which $\partial/\partial n$ is the normal derivative, K the cross-section of the tube and ∂K its boundary. The most general initial condition is of the form

$$c = c_0(\boldsymbol{r}, z) \qquad \text{at} \quad t = 0. \tag{2.6}$$

We apply a Fourier transform with respect to axial distance and a Laplace transform with respect to time:

$$\bar{c}(\boldsymbol{r}, k, s) = \mathscr{L}\mathscr{F} c = \int_0^\infty \int_{-\infty}^\infty c(\boldsymbol{r}, z, t) \exp(-\mathrm{i}kz - st)\, \mathrm{d}z\, \mathrm{d}t, \tag{2.7}$$

where $\mathscr{L}$ and $\mathscr{F}$ represent the Laplace and Fourier transforms respectively. The governing equation for the transformed concentration $\bar{c}$ is

$$\nabla_r^2 \bar{c} - \left(s + \mathrm{i}kv(\boldsymbol{r}) + k^2 P^{-2}\right)\bar{c} = -\mathscr{F} c_0. \tag{2.8}$$

Since the problem is linear in c, using the principle of superposition the solution may be expressed in terms of a Green's function $G(\boldsymbol{r}, z, t; \boldsymbol{r}_0)$ which satisfies the governing equation (2.4) and the initial condition

$$G(\boldsymbol{r}, z, 0; \boldsymbol{r}_0) = \pi\delta(\boldsymbol{r} - \boldsymbol{r}_0)\delta(z), \tag{2.9}$$

where δ is the Dirac delta function, so that the tracer is initially concentrated at the point $\boldsymbol{r} = \boldsymbol{r}_0$, $z = 0$. The choice of normalization implies that the z-integrated concentration per unit area of the cross-section tends to unity at long times. The general solution satisfying (2.6) can then be expressed in terms of this Green's function as

$$c(\boldsymbol{r}, z, t) = \pi^{-1} \int_{-\infty}^\infty \int_K G(\boldsymbol{r}, z - z_0, t; \boldsymbol{r}_0) c_0(\boldsymbol{r}_0, z_0)\, \mathrm{d}\boldsymbol{r}_0\, \mathrm{d}z_0. \tag{2.10}$$

A further simplification is achieved by expressing the solution for finite Péclet number in terms of that for infinite Péclet number. By inspection of (2.8), the relationship between these two functions in transform space is

$$\bar{G}(\boldsymbol{r}, k, s; \boldsymbol{r}_0) = \bar{G}_\infty(\boldsymbol{r}, k, s + k^2 P^{-2}; \boldsymbol{r}_0), \tag{2.11}$$

where G_∞ is the infinite-P Green's function (i.e. the solution obtained by neglecting axial molecular diffusion in (2.4)). Inverting, we find from elementary properties of

the transforms that

$$G(\boldsymbol{r},z,t;\boldsymbol{r}_0)=\frac{1}{2(\pi t)^{1/2}}\int_{-\infty}^{\infty}G_\infty(\boldsymbol{r},z-P^{-1}u,t;\boldsymbol{r}_0)\exp\left(-\frac{u^2}{4t}\right)\mathrm{d}u. \tag{2.12}$$

For the remainder of this section we restrict our attention to the case of infinite Péclet number. From (2.8), (2.9), the governing equation for $\bar{G}_\infty(\boldsymbol{r},k,s;\boldsymbol{r}_0)$ is

$$\nabla_r^2\bar{G}_\infty-(s+\mathrm{i}kv(\boldsymbol{r}))\,\bar{G}_\infty=-\pi\delta(\boldsymbol{r}-\boldsymbol{r}_0). \tag{2.13}$$

In order to invert the Fourier transform, we can use this equation to investigate the behaviour at the poles of $\bar{G}_\infty$ in the complex k-plane. If there is a pole at $k=k_n$, by definition $\bar{G}_\infty$ is asymptotically proportional to $(k-k_n)^{-1}$, and by inspection of (2.13), at leading order it satisfies a homogeneous version of the governing equation, with k set equal to k_n, and is subject to a boundary condition of the form (2.5). Now for each real value of s, non-trivial solutions of this governing equation exist for a sequence of values of k on the imaginary axis (with $\mathrm{Im}(k)\geqslant 0$ provided $s\geqslant 0$). We shall denote these eigenvalues, at which the poles of $\bar{G}_\infty$ lie, by $\mathrm{i}\ell_n(s)$, and the corresponding solutions of the homogeneous problem by $f_n(\boldsymbol{r};s)$, so the governing equations are written

$$\nabla_r^2 f_n-(s-\ell_n v(\boldsymbol{r}))\,f_n=0, \tag{2.14}$$

for $n=0,1,2,\ldots$. Since (2.14) is homogeneous, the normalization of f_n is arbitrary, but in the calculations below for Poiseuille flow, for definiteness we shall require f_n to be equal to unity on the axis of the tube.

To evaluate its residues at $k=\mathrm{i}\ell_n(s)$, we express $\bar{G}_\infty$ as the sum of the leading term just discussed and a remainder term ρ_n:

$$\bar{G}_\infty(\boldsymbol{r},k,s;\boldsymbol{r}_0)=C_n(\boldsymbol{r}_0;s)\frac{f_n(\boldsymbol{r};s)}{k-\mathrm{i}\ell_n(s)}+\rho_n(\boldsymbol{r},k,s;\boldsymbol{r}_0), \tag{2.15}$$

where C_n is the coefficient we wish to determine. Substituting (2.15) into (2.13), we find that the governing equation for ρ_n is

$$\nabla_r^2\rho_n-(s-\ell_n v(\boldsymbol{r}))\,\rho_n=\mathrm{i}C_n v(\boldsymbol{r})f_n-\pi\delta(\boldsymbol{r}-\boldsymbol{r}_0). \tag{2.16}$$

Now applying Green's theorem to the functions f_n and ρ_n and using the governing equations (2.14) and (2.16), together with the boundary conditions of the form (2.5) which apply to both functions, we obtain

$$\mathrm{i}C_n(\boldsymbol{r}_0;s)\int_K v(\boldsymbol{r}')f_n(\boldsymbol{r}';s)^2\,\mathrm{d}A'=\pi f_n(\boldsymbol{r}_0;s), \tag{2.17}$$

in which $\boldsymbol{r}'$ denotes the transverse integration variable and $\mathrm{d}A'$ the corresponding area element. With the resulting expression for C_n, (2.15) shows the asymptotic behaviour near the pole to be

$$\bar{G}_\infty(\boldsymbol{r},k,s;\boldsymbol{r}_0)\sim\frac{\pi f_n(\boldsymbol{r}_0;s)f_n(\boldsymbol{r};s)}{\mathrm{i}(k-\mathrm{i}\ell_n(s))\displaystyle\int_K v(\boldsymbol{r}')f_n(\boldsymbol{r}';s)^2\,\mathrm{d}A'} \tag{2.18}$$

as $k\to\mathrm{i}\ell_n(s)$. From this equation the residues can be deduced, and the Fourier transform inverted, to give an exact expression for the Laplace transform of the

Green's function:

$$\mathscr{L}G_\infty(\boldsymbol{r}, z, s; \boldsymbol{r}_0) = \pi \sum_{n=0}^{\infty} \frac{f_n(\boldsymbol{r}_0; s) f_n(\boldsymbol{r}; s)}{\int_K v(\boldsymbol{r}') f_n(\boldsymbol{r}'; s)^2 \, \mathrm{d}A'} \exp(-\ell_n(s) z). \tag{2.19}$$

We could continue by inverting the Laplace transform numerically. Instead, in the remainder of the paper we use (2.19) to derive asymptotic results by assuming z is large: first for the temporal moments of the concentration distribution (§3), and secondly for an asymptotic approximation for the time-variation of concentration at a fixed position (§§4,5).

3. Temporal moments of concentration

Many previous workers have characterized the development of dispersion by calculating the axial moments of the concentration distribution as functions of time. However, it is the temporal variation of concentration at a fixed position which is more frequently measured experimentally. We therefore present in this section some asymptotic results for the temporal moments of concentration when the dimensionless axial distance z is large.

3.1. *Relationship between finite-P and infinite-P moments*

For the axial moments, as can easily be shown from (2.11), the effect of axial molecular diffusion can be restored by convolving the infinite-P solution with a Gaussian that represents the purely diffusive solution. As a result, the relationships between finite-P and infinite-P axial moments are very simple (for comparison, they are given in equation (A 1)). The corresponding relationships for the temporal moments are rather more complicated, but may be derived as follows. The ith temporal moment (relative to $t = 0$) of the tracer concentration $G(\boldsymbol{r}, z, t; \boldsymbol{r}_0)$ is given in terms of the Laplace transform $\mathscr{L}G$ by

$$m_i(\boldsymbol{r}, z; \boldsymbol{r}_0) \equiv \int_0^\infty t^i G(\boldsymbol{r}, z, t; \boldsymbol{r}_0) \, \mathrm{d}t = (-1)^i \frac{\partial^i (\mathscr{L}G)}{\partial s^i}\bigg|_{s=0}. \tag{3.1}$$

From (2.11), we find that differentiation of the double transform $\bar{G}$ with respect to P^{-2} is equivalent to applying the operator $k^2 \partial/\partial s$. From basic properties of the Fourier transform, therefore, differentiation of the Laplace transform $\mathscr{L}G$ with respect to P^{-2} is equivalent to the application of $-\partial^3/\partial z^2 \, \partial s$. So (3.1) implies that

$$\frac{\partial^j}{\partial (P^{-2})^j} m_i = (-1)^{i+j} \frac{\partial^{i+3j} (\mathscr{L}G)}{\partial z^{2j} \, \partial s^{i+j}}\bigg|_{s=0} = \frac{\partial^{2j}}{\partial z^{2j}} m_{i+j}. \tag{3.2}$$

In order to make further progress it is necessary to neglect contributions to the moments corresponding to the $n \geqslant 1$ terms in (2.19), which decay exponentially as $z \to \infty$, and to make some assumptions about the z-dependence of the remaining contributions in the infinite-P case. We confine our attention to situations where (as in Taylor dispersion) for large z the moments of the temporal distribution are close to those of a Gaussian with mean z and variance proportional to z (in the sense that the ith moment about the mean differs from the Gaussian value by an $o(z^{i/2})$ quantity). We also assume that the non-decaying contributions to the moments about the mean are polynomial in z. With these assumptions, using (3.1) to express the

Fourier transforms of the m_i formally as Taylor series in P^{-2}, then inverting and using (3.2), we obtain

$$m_i = \sum_{j=0}^{i} \frac{1}{j!} P^{-2j} \frac{\partial^{2j}}{\partial z^{2j}} m_{i+j\,\infty} + o(1) \tag{3.3}$$

as $z \to \infty$, where the error term is in fact exponentially small. This equation implies that m_i depends on the infinite-P moments up to the $2i$th. However, if the relationship is re-formulated in terms of moments about the mean rather than about $t = 0$ we find that the ith finite-P moment depends only on the first i infinite-P moments. In this way, after some manipulation we obtain the finite-P temporal mean μ, variance σ^2 and third central moment v^3 in terms of their infinite-P counterparts:

$$\mu = \mu_\infty + 2P^{-2} + o(1), \tag{3.4a}$$

$$\sigma^2 = \sigma_\infty^2 + 2P^{-2}\left(\mu_\infty + 3\frac{\mathrm{d}}{\mathrm{d}z}\sigma_\infty^2\right) + 8P^{-4} + o(1), \tag{3.4b}$$

$$v^3 = v_\infty^3 + 2P^{-2}\left(3\sigma_\infty^2 + 3\mu_\infty\frac{\mathrm{d}}{\mathrm{d}z}\sigma_\infty^2 + 3\left[\frac{\mathrm{d}}{\mathrm{d}z}\sigma_\infty^2\right]^2 + 4\frac{\mathrm{d}}{\mathrm{d}z}v_\infty^3\right) + 12P^{-4}\left(\mu_\infty + 7\frac{\mathrm{d}}{\mathrm{d}z}\sigma_\infty^2\right) + 64P^{-6} + o(1) \tag{3.4c}$$

as $z \to \infty$, where once again the error terms are exponentially small.

3.2. *Infinite-P moments for Poiseuille flow*

The temporal moments for infinite P have been given in this approximation by Smith (1984) for a more general problem in which the cross-section and flow field can vary with z. In the z-independent case we are considering, the temporal moments can be found very easily from (2.14) by a regular, small-s perturbation calculation of series solutions for the eigenvalues ℓ_n and eigenfunctions f_n. The results follow by substitution into (2.19) and use of (3.1).

As an example we give the mean and the next two central moments of the temporal distribution for the special case of Poiseuille flow, confining ourselves as above to the non-decaying contributions, which correspond to ℓ_0. (Smith's result for the third moment is thereby slightly extended, to include the next term, which is independent of z but dependent on $\boldsymbol{r}$ and $\boldsymbol{r}_0$.) We express ℓ_0 and f_0 as power series in s:

$$\ell_0(s) = \sum_{j=0}^{3} \ell_{0j} s^j + O(s^4), \qquad f_0(\boldsymbol{r}; s) = \sum_{j=0}^{3} f_{0j}(\boldsymbol{r}) s^j + O(s^4). \tag{3.5}$$

Substituting these series into (2.14) we find that $\ell_{00} = 0$ and $f_{00} = 1$, and that the resulting governing equations are

$$\nabla_r^2 f_{0j} = f_{0j-1} - v(\boldsymbol{r}) \sum_{k=0}^{j-1} \ell_{0j-k} f_{0k}, \tag{3.6}$$

which with the boundary condition (2.5) defines a simple eigenvalue problem for ℓ_{0j} and f_{0j}. It is therefore straightforward to solve term by term. The series solution for ℓ_0 is found to be

$$\ell_0(s) = s - \tfrac{1}{48}s^2 + \tfrac{1}{1920}s^3 + O(s^4), \tag{3.7}$$

and the functions $f_{0i}(r)$ are given by

$$\left.\begin{aligned} f_{01}(r) &= \tfrac{1}{8}(r^4 - 2r^2), \\ f_{02}(r) &= \tfrac{1}{2304}(9r^8 - 40r^6 + 30r^4 + 24r^2), \\ f_{03}(r) &= \tfrac{1}{460800}(25r^{12} - 178r^{10} + 275r^8 + 300r^6 - 570r^4 - 120r^2), \end{aligned}\right\} \tag{3.8}$$

where we have chosen a in (2.1) to be the radius of the tube, so that $r = |r|$ is the distance from the axis as a fraction of the radius. Hence from (2.19) and (3.1) we deduce the temporal mean, variance and third central moment for the case where tracer is initially present at a distance r_0, and is observed at a distance r, from the axis:

$$\mu_\infty = z - \tfrac{1}{8} - f_{01}(r_0) - f_{01}(r) + o(1), \tag{3.9a}$$

$$\sigma^2_\infty = \tfrac{1}{24}z - \tfrac{11}{960} - \left(f_{01}(r_0)^2 - 2f_{02}(r_0)\right) - \left(f_{01}(r)^2 - 2f_{02}(r)\right) + o(1), \tag{3.9b}$$

$$\begin{aligned} \nu^3_\infty = \tfrac{1}{320}z - \tfrac{307}{537600} &- 2\left(f_{01}(r_0)^3 - 3f_{01}(r_0)f_{02}(r_0) + 3f_{03}(r_0)\right) \\ &-2\left(f_{01}(r)^3 - 3f_{01}(r)f_{02}(r) + 3f_{03}(r)\right) + o(1) \end{aligned} \tag{3.9c}$$

as $z \to \infty$. The error terms are exponentially small. For an arbitrary initial transverse distribution, the slowest decaying mode is a non-axisymmetric one proportional to $\exp(-4.16z)$. If the initial condition is axisymmetric, or the observed concentration is averaged axisymmetrically, this contribution is absent, and the slowest decaying mode is instead proportional to $\exp(-12.84z)$.

Equation (3.9) gives the temporal moments of the Green's function G_∞. Since the problem is linear, the superposition principle expressed by (2.10) allows us to evaluate straightforwardly the temporal moments, for an arbitrary initial distribution over the cross-section $z = 0$, and an arbitrary transverse weighting of the observed concentration. These are obtained by replacing each of the functions $f_{0i}(r_0)$ wherever it appears in (3.9) by a cross-sectional average, weighted by the initial distribution, and likewise each $f_{0i}(r)$ by a cross-sectional average, weighted by the transverse distribution of sampling. (Note that this is not the same as obtaining weighted averages of the nonlinear combinations of $f_{0i}(r_0)$ and $f_{0i}(r)$ that occur in (3.9)!) As (2.10) implies, a second stage of averaging with respect to z allows the moments to be calculated for an arbitrary initial radial and axial distribution.

The most commonly considered initial condition is a uniform distribution of tracer over the cross-section at $z = 0$, with a density per unit cross-sectional area equal to 1. In this case, for an area-weighted average of the observed concentration, we obtain the moments, denoted by a subscript a,

$$\mu_{\infty a} = z + \tfrac{1}{24} + o(1), \quad \sigma^2_{\infty a} = \tfrac{1}{24}z - \tfrac{1}{720} + o(1), \quad \nu^3_{\infty a} = \tfrac{1}{320}z - \tfrac{61}{138240} + o(1) \tag{3.10a–c}$$

as $z \to \infty$. Another average which has sometimes been considered is the flow-weighted (or 'cup-mixed') average. In the infinite-P case, since axial diffusion is negligible, the flow-weighted average of concentration is directly proportional to the axial flux of tracer. For the same initial condition, the moments of this average, denoted by a subscript f, are

$$\mu_{\infty f} = z + \tfrac{1}{48} + o(1), \quad \sigma^2_{\infty f} = \tfrac{1}{24}z - \tfrac{23}{11520} + o(1), \quad \nu^3_{\infty f} = \tfrac{1}{320}z - \tfrac{1367}{3870720} + o(1) \tag{3.11a–c}$$

as $z \to \infty$. The corresponding spatial moments are given for comparison in (A 6)–(A 8a–c).

In §6.1 below we derive from these results the moments in dimensional form, when the Péclet number is finite. As discussed there, the naive calculation of temporal

moments using Taylor's Gaussian approximation (Levenspiel & Smith 1957) fails to predict the correct behaviour for $v_{\infty a}^3$ (giving instead the spurious value $\frac{1}{192}z + O(1)$). This discrepancy was discussed by Chatwin (1980), who showed that the skewness resulting from the time-evolution of the Gaussian as it passes the measurement point is of the same order as the skewness of the axial distribution, which is omitted in the naive approach. The latter is positive in the axial sense, and therefore makes a negative contribution to the temporal skewness, but this is outweighed by the larger, positive contribution due to time evolution. (In Chatwin's equation (20), for Poiseuille flow the constant β may be evaluated by comparison with his previous (1970) asymptotic solution as $\frac{1}{10}\sqrt{2}$, but the sign of the second term representing axial skewness should be reversed.) Because the standard deviation is asymptotically proportional to $z^{1/2}$, the coefficient of skewness $v_\infty^3/\sigma_\infty^3$ tends to zero as z increases, consistent with the approach to a Gaussian profile.

4. Asymptotic approximation for the temporal concentration variation for large z

We now return to the case where the cross-section of the tube and the axial flow profile are arbitrary, and seek a large-z asymptotic approximation for the Green's function $G_\infty(\boldsymbol{r}, z, t; \boldsymbol{r}_0)$. It is necessary also to stipulate the behaviour of t as z tends to infinity. Viewed as a function of time, Taylor's (1953) Gaussian approximation is asymptotically valid provided $z^{-1/2}(t-z)$ is of order unity as $z \to \infty$. Instead, we seek an approximation which is uniformly valid over the whole range of t, by defining a rescaled version of t,

$$\tau = z^{-1}(t - z), \tag{4.1}$$

and considering τ to be fixed as $z \to \infty$. (In the Taylor régime, this variable is asymptotically small, of order $z^{-1/2}$.) From (2.19), in terms of τ, the Green's function is given by

$$G_\infty(\boldsymbol{r}, z, t; \boldsymbol{r}_0) = \frac{1}{2\pi \mathrm{i}} \sum_{n=0}^{\infty} \int_{\mathscr{C}_n} F_n(\boldsymbol{r}_0, \boldsymbol{r}; s) \exp\{(s\tau + s - \ell_n(s))\, z\}\, \mathrm{d}s, \tag{4.2}$$

in which

$$F_n(\boldsymbol{r}_0, \boldsymbol{r}; s) = \frac{\pi f_n(\boldsymbol{r}_0; s) f_n(\boldsymbol{r}; s)}{\displaystyle\int_K v(\boldsymbol{r}') f_n(\boldsymbol{r}'; s)^2 \, \mathrm{d}A'} \tag{4.3}$$

and the $\mathscr{C}_n$ are suitably chosen contours of integration for the inversion of the Laplace transform. Investigation of the behaviour of F_n and ℓ_n in the complex s-plane (Appendix B) shows that when z is large the leading-order solution (with errors exponentially small in z) is obtained from the first term of the sum in (4.2), with the contour $\mathscr{C}_0$ chosen to pass through the saddle point of the exponent. This lies on the real axis at the value $s = s_\tau$ satisfying

$$\ell_0'(s_\tau) - 1 = \tau. \tag{4.4}$$

With this choice of contour the dominant contributions to the integral arise from a small neighbourhood of $s = s_\tau$, of size $z^{-1/2}$, so by rescaling the integration variable as $z^{1/2}(s - s_\tau)$, expanding F_0 and ℓ_0 locally in Taylor series and evaluating the resulting

integrals we find straightforwardly that

$$G_\infty(\boldsymbol{r}, z, t; \boldsymbol{r}_0) = \frac{\mathrm{e}^{-z\phi(\tau)}}{2(\pi\kappa z)^{1/2}} \left(\alpha(\boldsymbol{r}_0, \boldsymbol{r}, \tau) + z^{-1}\beta(\boldsymbol{r}_0, \boldsymbol{r}, \tau) + O(z^{-2})\right), \tag{4.5}$$

as $z \to \infty$, in which the (positive) constant κ is given by

$$\kappa = -\tfrac{1}{2}\ell_0''(0), \tag{4.6}$$

and the functions ϕ, α and β are defined in terms of $F_0(\boldsymbol{r}_0, \boldsymbol{r}; s)$, $\ell_0(s)$ and their s-derivatives, all evaluated at $s = s_\tau$, by

$$\phi = [\ell_0 - s\tau - s]\Big|_{s=s_\tau}, \tag{4.7a}$$

$$\alpha = \left[\left(\frac{2\kappa}{|\ell_0''|}\right)^{1/2} F_0\right]\Bigg|_{s=s_\tau}, \tag{4.7b}$$

$$\beta = \left[-\left(\frac{\kappa}{2|\ell_0''|^3}\right)^{1/2}\left\{F_0'' + \frac{(F_0'\ell_0''' + \frac{1}{4}F_0\ell_0'''')}{|\ell_0''|} + \frac{5F_0\ell_0'''^2}{12|\ell_0''|^2}\right\}\right]\Bigg|_{s=s_\tau}, \tag{4.7c}$$

in which the prime denotes differentiation with respect to s.

Apart from the explicit appearance of z in (4.5), the Green's function depends on the rescaled time τ and transverse position through the three functions $\phi(\tau)$, $\alpha(\boldsymbol{r}_0, \boldsymbol{r}, \tau)$ and $\beta(\boldsymbol{r}_0, \boldsymbol{r}, \tau)$, which depend on the cross-sectional geometry and flow field, and in general must be determined by numerical solution of (2.14) and its s-derivatives. Since the problem is linear, the superposition principle expressed by (2.10) allows us to deduce from (4.5) the solution for an arbitrary initial distribution over the cross-section $z = 0$, and an arbitrary weighted integral of the measured concentration, by evaluating appropriately weighted cross-sectional integrals of the Green's function with respect to $\boldsymbol{r}_0$ and $\boldsymbol{r}$. Now the general solution depends on $\boldsymbol{r}_0$ and $\boldsymbol{r}$ only through α and β, and each of these depends linearly on F_0. In turn, by inspection of (4.3), F_0 depends linearly on each of $f_0(\boldsymbol{r}_0; s)$ and $f_0(\boldsymbol{r}; s)$ (and there is symmetry between the initial and final positions $\boldsymbol{r}_0$ and $\boldsymbol{r}$). It follows that the required integrals can be obtained simply by replacing $f_0(\boldsymbol{r}_0; s)$ in (4.3) with a cross-sectional average weighted by the initial transverse distribution, and $f_0(\boldsymbol{r}; s)$ by an average using the same weighting that is applied to the measured concentration. The resulting approximation for the concentration can be expressed as a function of z and t, in terms of three functions of τ alone, namely $\phi(\tau)$ and the appropriate cross-sectional integrals of α and β. Finally, as (2.10) shows, the solution corresponding to an arbitrary initial radial and axial distribution can be evaluated by means of a second stage of integration with respect to z.

As mentioned above, the Gaussian approximation due to Taylor (1953) is applicable in the central region where τ is small, of order $z^{-1/2}$. Substituting a quadratic small-s_τ approximation for ℓ_0 into (4.4) and (4.7a), and using (4.6), we find that $\phi \sim \frac{1}{4}\kappa^{-1}\tau^2$. Since, also from (4.6), $|\ell_0''| \to 2\kappa$ and, from (3.5), $F_0 \to 1$ as $s \to 0$, we find also that $\alpha \to 1$ as $\tau \to 0$. Combining these results we recover from (4.5) the leading-order solution

$$G_\infty(\boldsymbol{r}, z, t; \boldsymbol{r}_0) \sim \frac{1}{2(\pi\kappa z)^{1/2}} \exp\left(-\frac{(t-z)^2}{4\kappa z}\right), \tag{4.8}$$

for $t - z = O(z^{1/2})$ as $z \to \infty$. Since $z \sim t$ in this limit, this Gaussian distribution is at leading order the temporal equivalent of Taylor's translating, dispersing Gaussian

axial concentration distribution. The constant κ is to be identified with the dimensionless value of the dispersion coefficient (which in dimensional terms is $\kappa P^2 D$). The departures from the Gaussian form (small in this region) are represented by the difference of ϕ from its leading quadratic term $\frac{1}{4}\kappa^{-1}\tau^2$, the difference of α from unity, and the presence of β. It is straightforward to calculate series approximations for ϕ, α and β when τ is small, and so to improve the approximation (4.8). Note that including higher powers of τ in the series for ϕ in the exponent actually enlarges the region of asymptotic validity: including powers up to τ^n means the approximation remains asymptotic until $t - z$ is comparable with $z^{1-1/n}$. This is in contrast to previous improvements of Taylor's approximation (Chatwin 1970; Smith 1985; Stokes & Barton, 1990), which leave the exponential unchanged, and so remain limited to $t - z = O(z^{1/2})$, as discussed in §5.1.

5. The development of dispersion in Poiseuille flow

We now apply the general solution derived in §4 to the particular case of Poiseuille flow. It follows immediately from (3.7) and (4.6) that the constant κ appearing in (4.5) is given by

$$\kappa = \tfrac{1}{48}. \tag{5.1}$$

As discussed above, this is the dimensionless value of Taylor's (1953) dispersion coefficient.

In the remainder of the section we consider departures from the temporal version of Taylor's approximation, (4.8), during the development of dispersion. First we give asymptotic approximations for the functions ϕ, α and β, applicable: (i) in the central region where $\tau \ll 1$; (ii) near the beginning of the transient (which is found to correspond to $\tau + \frac{1}{2} \ll 1$) and (iii) in the tail, where $\tau \gg 1$. We then show exact numerical results for ϕ, α and β and the form of the asymptotic approximation (4.5) for the temporal concentration distribution at particular values of z.

5.1. *Behaviour for small* τ

Series approximations when τ is small can be obtained by applying (3.7) in (4.4) and then using (4.3) and (4.7). The results are

$$\phi(\tau) = 12\tau^2 - \tfrac{36}{5}\tau^3 + \tfrac{4197}{350}\tau^4 + O(\tau^5), \tag{5.2a}$$

$$\begin{aligned}\alpha(\boldsymbol{r}_0, \boldsymbol{r}, \tau) = 1 &- \left[\tfrac{39}{10} + 24\left(f_{01}(r) + f_{01}(r_0)\right)\right]\tau \\ &+ \left[\tfrac{1287}{140} + 576\left(\tfrac{1}{5}f_{01}(r) + \tfrac{1}{5}f_{01}(r_0) + f_{01}(r)f_{01}(r_0)\right.\right. \\ &\left.\left. + f_{02}(r) + f_{02}(r_0)\right)\right]\tau^2 + O(\tau^3),\end{aligned} \tag{5.2b}$$

$$\begin{aligned}\beta(\boldsymbol{r}_0, \boldsymbol{r}, \tau) = &-\tfrac{907}{4480} - \tfrac{39}{10}\left(f_{01}(r) + f_{01}(r_0)\right) \\ &-24\left(f_{01}(r)f_{01}(r_0) + f_{02}(r) + f_{02}(r_0)\right) + O(\tau),\end{aligned} \tag{5.2c}$$

in which the functions f_{0i}, defined by (3.8), are the same as those appearing in equations (3.9) for the temporal moments. These results for α and β express the dependence of G_∞ on the initial position r_0 and the sampling position r, and are consequently rather unwieldy. For specified initial conditions and cross-sectionally averaged concentration, however, they are much simpler. The most commonly considered initial condition is a uniform distribution across the cross-section $z = 0$,

with a cross-sectional density per unit area equal to 1; to find the corresponding form of (5.2), the $f_{0i}(r_0)$ must be replaced by their (area-weighted) cross-sectional averages. If, in addition, we consider the area-weighted cross-sectional average of the observed concentration, denoted by $\langle \ldots \rangle$, the $f_{0i}(r)$ in (5.2) must be replaced similarly, we obtain

$$\langle \alpha \rangle(\tau) = 1 + \tfrac{1}{10}\tau + \tfrac{25}{28}\tau^2 + O(\tau^3), \quad \langle \beta \rangle(\tau) = -\tfrac{89}{13440} + O(\tau). \tag{5.3}$$

The other form of sampling commonly considered is the flow-weighted (or 'cup-mixed') average. For the uniform initial cross-sectional distribution, by replacing the $f_{0i}(r)$ instead by flow-weighted cross-sectional averages, we obtain

$$\langle v\alpha \rangle(\tau) = 1 - \tfrac{2}{5}\tau + \tfrac{87}{70}\tau^2 + O(\tau^3), \quad \langle v\beta \rangle(\tau) = -\tfrac{11}{4480} + O(\tau). \tag{5.4}$$

In §6.2, these equations are used to derive in dimensional form an approximation for the tracer concentration near its peak.

5.2. *Behaviour near* $\tau = -\frac{1}{2}$

In the absence of axial molecular diffusion, the minimum time of arrival of tracer a distance z downstream is determined by the peak value of axial velocity, which in Poiseuille flow occurs on the axis and is equal to twice the mean axial velocity. So in dimensionless terms the onset of the observed concentration transient occurs at $t = \frac{1}{2}z$, i.e. at $\tau = -\frac{1}{2}$, and the first appearance of tracer is at the axis. The leading-order behaviour just after the onset is expressed by the asymptotic forms of α and ϕ as $\tau \to -\frac{1}{2}$. In Appendix C, §C.1 we outline the derivation of the asymptotic solution of (2.14) in the limit $s \to \infty$, which is found to correspond to $\tau \to -\frac{1}{2}$. This gives

$$\phi(\tau) = \frac{(\tau+1)^2}{\tau+\frac{1}{2}} - \frac{4(\tau+1)^3}{(\tau+\frac{1}{2})^2} \exp\left(-\frac{\tau+1}{\tau+\frac{1}{2}}\right) + \ldots \tag{5.5}$$

as $\tau + \frac{1}{2} \to 0$, in which the errors are algebraically smaller than the second term. The function $f_0(r, s_\tau)$, expressing the leading-order radial variation of concentration, is by definition equal to unity at the axis, but decays rapidly away from $r = 0$. In Appendix C, §C.1 it is shown that

$$f_0(r, s_\tau) \sim \begin{cases} \exp\left(-\dfrac{\tau+1}{2\tau+1} r^2\right) & \text{for } 1 - r \gg \tau + \frac{1}{2}, \quad (5.6a) \\ 2\exp\left(-\dfrac{\tau+1}{2\tau+1}\right) \cosh\left(\dfrac{1-r}{2\tau+1}\right) & \text{for } 1 - r = O(\tau + \frac{1}{2}); \quad (5.6b) \end{cases}$$

the relative error is exponentially small in (5.6*a*), but only algebraically small in (5.6*b*). In terms of this function,

$$\alpha(r_0, r, \tau) \sim \frac{(\tau+1)^2 f_0(r_0, s_\tau) f_0(r, s_\tau)}{4\sqrt{3}(\tau+\frac{1}{2})^{5/2}}, \tag{5.7}$$

with an exponentially small relative error. (An expression for $\beta(r_0, r, \tau)$ can also be found using (4.7c), but it is rather cumbersome, and takes different forms in the two regions.)

For the cross-sectionally uniform initial condition considered above, simpler approximations for the temporal concentration variation follow. Integrating (5.7) with

respect to r_0 and using (4.5) gives

$$c(r,z,t) \sim \frac{(\tau+1)f_0(r,s_\tau)\mathrm{e}^{-z\phi(\tau)}}{(\pi z)^{1/2}(\tau+\frac{1}{2})^{3/2}}. \tag{5.8}$$

By carrying out further integrations with respect to r, we obtain the area- and flow-weighted cross-sectional averages of concentration:

$$\langle c\rangle(z,t) \sim \frac{2\mathrm{e}^{-z\phi(\tau)}}{(\pi z)^{1/2}(\tau+\frac{1}{2})^{1/2}}, \quad \langle vc\rangle(z,t) \sim \frac{4|\tau|\mathrm{e}^{-z\phi(\tau)}}{(\pi z)^{1/2}(\tau+\frac{1}{2})^{1/2}(\tau+1)} \tag{5.9a,b}$$

as $\tau \to -\frac{1}{2}$. As is true throughout this section, τ is assumed to be held fixed as $z \to \infty$, and (5.8) and (5.9) are approximations appropriate when in addition $\tau+\frac{1}{2}$ is small. In practice these approximations are subject to two sources of error. The small-$(\tau+\frac{1}{2})$ approximations (5.5), (5.7) involve exponentially small errors. In addition the large-z approximation involves errors that are algebraically small in z, namely $z^{-1}\beta$ and higher-order terms. Estimation of β as $\tau \to -\frac{1}{2}$ shows that for the averaged concentrations (5.9a,b), and on the axis $r=0$, the relative size of the correction term is $z^{-1}(\tau+\frac{1}{2})^2$ or less, so that it remains small (Appendix C, §C.1). However, for other values of r, for a given value of z, (5.8) can break down when $\tau+\frac{1}{2}$ becomes sufficiently small, so that in practice, the closer one comes to the onset, the larger z must be for the approximation to remain accurate. It is interesting to note that if ϕ is set equal to the leading term in (5.5), the asymptotic approximation (5.9a) (valid when $z \gg 1$ and $\tau+\frac{1}{2} \ll 1$) is identical with the first term of Lighthill's (1966) solution for $\langle c\rangle$ near the 'leading edge' of the tracer distribution at short times (valid, in our notation, when z and $\tau+\frac{1}{2}$ are both small and are comparable with each other).

5.3. *Behaviour as* $\tau \to \infty$

For the long-time behaviour, i.e. the limit $\tau \to \infty$, we seek an asymptotic approximation for ℓ_0 and f_0 in the limit $s \to -\infty$. The derivation is outlined in Appendix C, §C.2, and leads to

$$\ell_0(s) = -\lambda_0(-s)^{3/2} - \lambda_1(-s) - \lambda_2(-s)^{1/2} - \lambda_3 + O(-s)^{-1/2}, \tag{5.10}$$

where the λ_i are constants whose values are given in (C 17). It can then be deduced from (5.10) that the asymptotic form of the exponent function $\phi(\tau)$ for large τ is

$$\phi(\tau) = \phi_0\tau^3 + \phi_1\tau^2 + \phi_2\tau + \phi_3 + O(\tau^{-1}), \tag{5.11}$$

where the constants ϕ_i are given in (C 18).

The function $f_0(r,s_\tau)$ describing the radial variation of concentration is, by definition, of order unity near the axis, but rises to become exponentially larger at the wall. The solution takes a different form in each of three radial regions, and can be expressed as

$$f_0(r,s_\tau) \sim \begin{cases} I_0\left(\dfrac{4}{3\sqrt{3}}\lambda_0^{-1}\tau^{3/2}r\right) & \text{for } r = O(\tau^{-3/2}), \\ \dfrac{3^{3/4}\lambda_0^{1/2}}{2^{3/2}\pi^{1/2}r^{1/2}(1-r^2)^{1/4}\tau^{3/4}}\exp(\theta(r,\tau)) & \text{for intermediate } r, \\ \dfrac{3^{1/2}\lambda_0^{1/3}}{2^{1/3}\tau^{1/2}}\exp(\theta(1,\tau))\mathrm{Ai}\left(2^{-4/3}\lambda_0^{-2/3}\left\{\frac{8}{3}\tau(1-r)-1\right\}\right) & \text{for } 1-r = O(\tau^{-1}), \end{cases} \tag{5.12}$$

in which I_0 denotes a modified Bessel function, Ai the Airy function, and

$$\theta(r,\tau) = \frac{2}{3\sqrt{3}}\lambda_0^{-1}\left(r(1-r^2)^{1/2} + \sin^{-1} r\right)\tau^{3/2} + \frac{1}{2\sqrt{3}}\lambda_0^{-1}\left((2-\lambda_1)r(1-r^2)^{1/2} + (1-\lambda_1)\sin^{-1} r\right)\tau^{1/2}. \tag{5.13}$$

In terms of the function f_0, we find that

$$\alpha(r_0, r, \tau) \sim \frac{2\tau^{7/2} f_0(r_0, s_\tau) f_0(r, s_\tau) \exp(-2\theta(1,\tau))}{81\sqrt{3}\lambda_0^3 Q_0}, \tag{5.14}$$

where Q_0 is a constant given by (C 22).

For the special case where tracer is initially uniformly distributed over the cross-section with a density per unit area of 1, the cross-sectionally averaged concentration in the tail is

$$\langle c\rangle(z,t) = \frac{Q_1^2 \tau^{1/2} e^{-z\phi(\tau)}}{3\lambda_0 Q_0 (\pi z)^{1/2}}\left(1 + O(\tau^{-1}, z^{-1}\tau^{-3})\right), \tag{5.15}$$

in which Q_1 is a constant given by (C 23*a*). For the same initial conditions, the flow-weighted version is

$$\langle vc\rangle(z,t) = \frac{2^{1/3} Q_1 Q_2 \tau^{-1/2} e^{-z\phi(\tau)}}{\lambda_0^{1/3} Q_0 (\pi z)^{1/2}}\left(1 + O(\tau^{-1}, z^{-1}\tau^{-3})\right), \tag{5.16}$$

in which Q_2 is a constant given by (C 23*b*).

As in §5.2, the correction function β takes a rather complicated form, and will not be given here. In this case, however, examination of the limiting form of β as $\tau \to \infty$ shows that it is the same order as α, so that the leading term of (4.5) remains valid throughout the tail.

The $\tau \to \infty$ approximation (5.11)–(5.16) may be compared with another short-time approximation for $\langle c\rangle$, for the 'trailing edge' of the axial tracer distribution, due to Stokes & Barton (1990). This is valid when z is comparable with $t^{3/2}$ and t is small, and consists of a series solution (their (28)), of which all but the first term are exponentially small in our large-z régime. The first term is related to our solution, but the relationship is not as close as for the 'leading-edge' approximation discussed in §5.2. The term, if the large-z limit is taken, contains an exponential factor equal to $\exp(-\phi_0 z\tau^3)$ in our notation. But the remaining terms of (5.11), which would be small in the short-time régime, are absent, and the factors multiplying the exponentials do not seem to be equivalent.

5.4. *Numerical results*

In this subsection we illustrate the behaviour of the asymptotic approximation (4.5) for Poiseuille flow, and compare it with both the numerical solutions of Shankar & Lenhoff (1991) and the simpler approximations for particular ranges of τ just presented. First we show computed results for the functions ϕ, α and β, which are necessary to evaluate the asymptotic approximation (4.5), together with f_0, which expresses the radial variation of concentration. We confine ourselves to values of τ up to unity, since in practice when z is sufficiently large for the approximation to be accurate, the concentration is very small beyond this point.

In figure 1 the function ϕ, which appears in the exponent of (4.5), is shown. Near the origin, ϕ is quadratic at leading order, but away from the origin it exhibits a skewed form, tending to infinity both at the onset of the transient at $\tau \to -\frac{1}{2}$ and

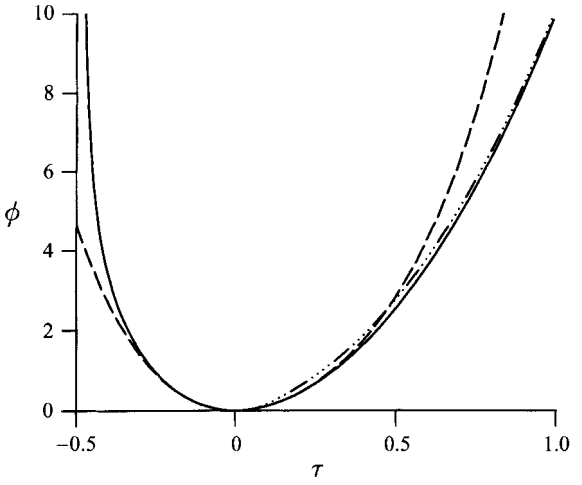

FIGURE 1. The function ϕ that appears in the exponent of (4.5), as a function of τ. In addition to the exact curve, obtained numerically —— we show two asymptotic approximations: the three-term series (5.2*a*) valid for small τ — — —; the four-term approximation (5.11) valid for large τ —·····—·····. NB On the scale shown, the two-term approximation (5.5), valid when τ is close to $-\frac{1}{2}$, is indistinguishable from the exact curve up to about $\tau = -0.1$, and has not been shown.

(as a cubic) as $\tau \to \infty$, so that the concentration must tend to zero in both these limits. At the leading order, the approximation (4.5) for a fixed value of τ depends on z through a multiplicative factor $z^{-1/2}$, and through the exponential $\exp(-z\phi(\tau))$. The form of the latter means that, as z is increased, the region near $\tau = 0$ for which the concentration is significant is progressively reduced. Finally, when z is large, the quadratic approximation for ϕ is appropriate and the expression (4.8), corresponding to Taylor's solution, is obtained.

For comparison with the exact curve, figure 1 also shows small-τ (quartic) and large-τ (cubic) asymptotic approximations for ϕ. The approximation (5.5) for $\tau \to -\frac{1}{2}$ is not shown because it lies too close to the exact curve to be seen clearly (within 4% for $\tau < -0.14$); unfortunately its accuracy seems to be somewhat fortuitous, as the corresponding approximations for α and β break down far earlier.

Since the exponential in (4.5) does not depend on either the distance r_0 from the axis at which tracer is released or the distance r at which concentration is measured, at leading order the dependence on both r_0 and r is expressed by α, which is proportional to the product $f_0(r_0; s_\tau) f_0(r; s_\tau)$. In figure 2 this radial dependence is illustrated, for several values of τ, by showing a version of $f_0(r; s_\tau)$, rescaled so that its (area-weighted) cross-sectional average is unity, as a function of r. Early in the transient near $\tau = -\frac{1}{2}$, the higher velocities near the axis mean that tracer lies mainly in the neighbourhood of $r = 0$. Subsequently it becomes more uniform, until in the Taylor régime when τ is small (of order $z^{-1/2}$), the radial variation is also small and of the same order. Conversely, at longer times, the tracer remaining is found mostly near the wall where flow is slowest.

For the remainder of this subsection we shall assume that tracer is initially distributed uniformly over the cross-section of the tube at $z = 0$ with cross-sectional density per unit area equal to 1, so that all quantities are (area-weighted) integrals with respect to r_0. Four different weightings will be used for integration with respect to the observation position r, so that the results express an area-weighted average,

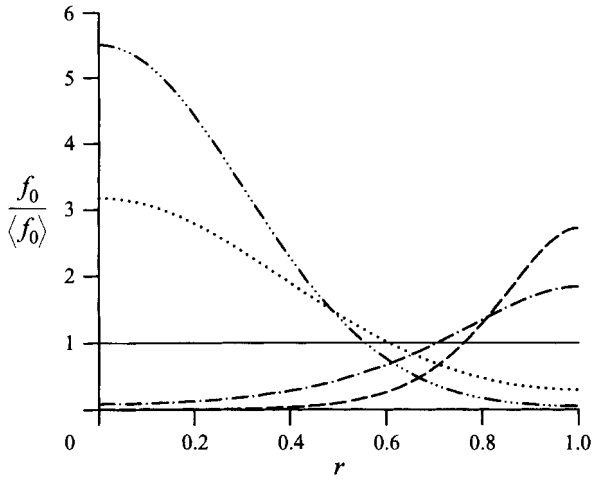

FIGURE 2. Leading-order variation of concentration with radius r between the axis ($r = 0$) and the wall ($r = 1$), normalized so that the (area-weighted) cross-sectional average is unity. The radial distribution is shown for different values of the dimensionless time: —·····—·····, $\tau = -0.45$; ·····, $\tau = -0.4$; ——, $\tau = 0$; -·-·-, $\tau = 1$; – – –, $\tau = 2$.

a flow-weighted average, concentration on the axis and concentration at the wall. However, in view of the symmetry of (4.5) between r_0 and r, it should be noted that the results shown can equally be viewed as the area-weighted observations resulting from non-uniform initial distributions.

For the function α, which multiplies the exponential function in (4.5), figure 3 shows the four weighted integrals, just referred to, as a function of τ. For clarity, the simpler approximations for particular ranges of τ are not shown; they are, however, incorporated in the results for the concentration profile shown in figure 5 below. The behaviour shown is consistent with that illustrated in figure 2, in that, for $\tau < 0$, α decreases monotonically from the axis to the wall, and for $\tau > 0$ the opposite is true. The flow weighting gives preference to the region near the axis, and so gives a larger value of α than the area weighting. (This behaviour will be somewhat modified by the β term and higher-order corrections.) Note that in both the limits $\tau \to -\frac{1}{2}$ and $\tau \to \infty$, some of these integrals tend to infinity and some to zero; mathematically, it is the behaviour of ϕ, not α, which forces the concentration to tend to zero.

The behaviour of β, shown in figure 4, is rather more complicated. All the curves begin from zero at $\tau = -\frac{1}{2}$, and after about $\tau = -0.2$, the values of β are small and vary only gradually: for this reason the figure shows the curves only up to $\tau = 0$. In contrast, soon after the onset of the transient, the curves exhibit rapid variation: the area-weighted and flow-weighted averages both show sharp maxima, the value at the wall a sharp minimum, and the value on the axis a maximum quickly followed by a minimum. Note, however, that the absolute values of the functions remain fairly small, and it is only for quite small values of z that they are important, both because β is multiplied by z^{-1} in (4.5) and because as z increases the neighbourhood of $\tau = 0$ over which the concentration is significant decreases.

As an example of how α, β and ϕ are combined using (4.5) to give an asymptotic approximation for the variation of concentration with time at a fixed axial position, we show in figure 5 the flow-weighted average of concentration at $z = 0.3$. The present approximate solution is compared with the numerical results of Shankar

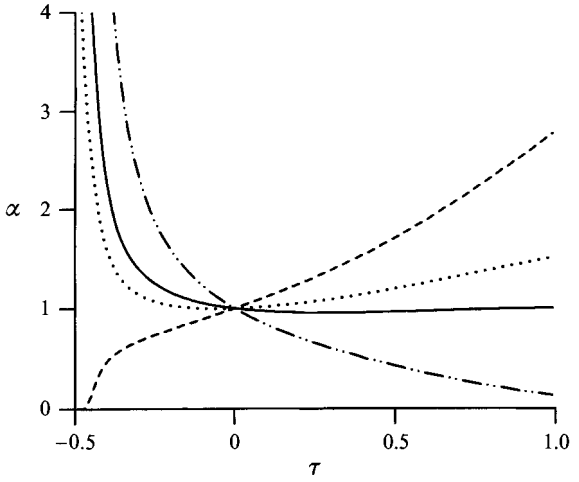

FIGURE 3. Cross-sectional integrals of the leading-order coefficient α, appearing in (4.5), as a function of τ. The functions are integrated with respect to r_0 as appropriate when the tracer substance is initially distributed uniformly over the cross-section. Weighted integrals with respect to r are then obtained, corresponding to: —··—, measurement on the axis $r = 0$; —— a flow-weighted cross-sectional average; ·····, an area-weighted cross-sectional average; – – –, measurement at the wall $r = 1$.

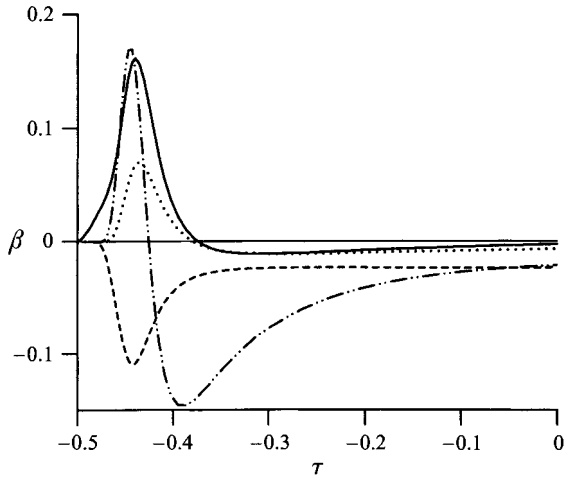

FIGURE 4. Cross-sectional integrals of the leading-order coefficient β, appearing in (4.5), as a function of τ. The functions are integrated with respect to r_0 as appropriate when the tracer substance is initially distributed uniformly over the cross-section. Weighted integrals with respect to r are then obtained, corresponding to: —··—··, measurement on the axis $r = 0$; ——, a flow-weighted cross-sectional average; ·····, an area-weighted cross-sectional average; – – –, measurement at the wall $r = 1$. Note that the time range is restricted to negative values of τ.

& Lenhoff (1991) for the same problem. Considering that the approximation is formally valid in the limit $z \to \infty$, the agreement between the two is surprisingly good. In particular, the twin-peaked profile characteristic of developing Taylor dispersion is reproduced: the first peak occurs soon after $t = 0.15$ and represents tracer advected by rapidly moving fluid near the axis; the second occurs just before $t = 0.3$ and corresponds to slower advection with a speed close to the cross-sectional

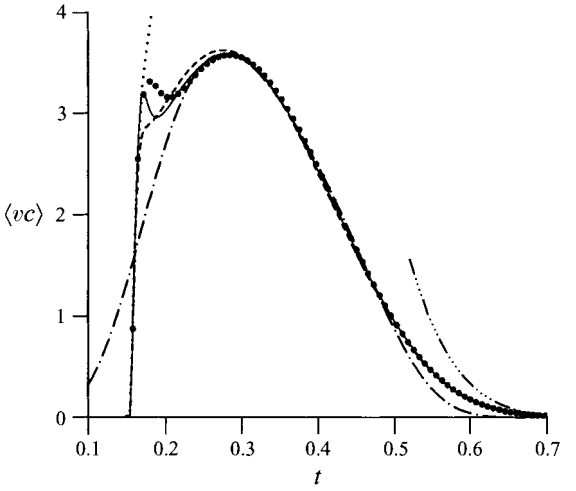

FIGURE 5. The flow-weighted cross-sectional average of concentration as a function of dimensionless time t, at a dimensionless distance $z = 0.3$ downstream of the point of release, assuming a uniform initial distribution over the cross section. In addition to the numerical results due to Shankar & Lenhoff (1991) (• • •) we show the asymptotic approximation (4.5) with ϕ, α and β computed exactly (——). Also shown are the simpler approximations: – – –, (i) leading-order version of (4.5), with β omitted; · · · · · ·, (ii) approximation for $\tau \to -\frac{1}{2}$, obtained from (5.5), (5.9*b*) and (C 7); – · – · –, (iii) small-τ approximation, obtained from (5.2*a*) and (5.4); – · · · · – · · · ·, (iv) large-τ approximation, obtained from (5.11) and (5.16).

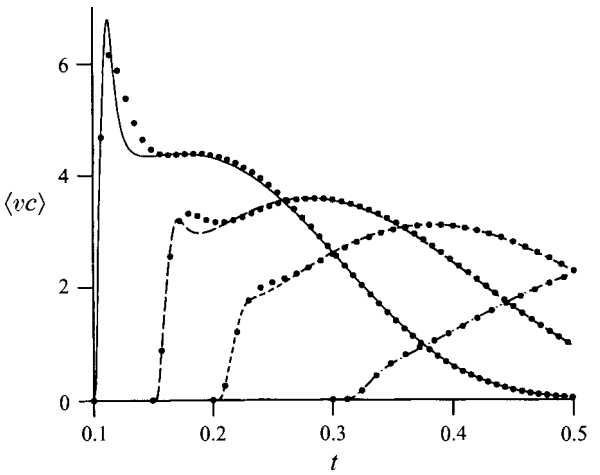

FIGURE 6. The flow-weighted cross-sectional average of concentration as a function of dimensionless time t, at several values of the dimensionless downstream distance z, assuming a uniform initial distribution over the cross-section. The asymptotic approximation (4.5) is shown together with numerical results due to Shankar & Lenhoff (1991) (• • •): ——, $z = 0.2$; — — —, $z = 0.3$; – – – –, $z = 0.4$; – · – · – · –, $z = 0.6$.

average. At larger distances, of course, the second peak becomes dominant as Taylor dispersion develops. The main deficiency of the asymptotic approximation is that the initial peak is predicted to be too narrow, and its height is somewhat underestimated. (Comparisons with numerical results for other values of z are given below, in figure 6.)

For further comparison, figure 5 also shows several simpler approximations. The leading-order version of (4.5), with the β term omitted, is shown. This omission results in the disappearance of the initial peak (although a residual 'shoulder' is still evident), and a slight compensatory increase of the second peak. Curves based on asymptotic approximations for ϕ, α and β are also shown. While each describes the curve within a certain range, at this value of z their deficiencies are quite serious. The small-τ approximation describes the second peak and its decline quite well, but wholly lacks the initial peak, and predicts spurious positive concentrations before the onset at $t = 0.15$. On the other hand the initial rise, up to just before the first peak, is accurately described by the $\tau \to -\frac{1}{2}$ approximation, but this continues to increase steeply beyond the peak. The large-τ approximation retains a significant error over the whole range shown, although beyond about $t = 0.6$ it is an improvement on the small-τ curve.

The evolution of the temporal profile with downstream distance is illustrated in figure 6. Once again the solutions computed by Shankar & Lenhoff (1991) are shown, together with the full asymptotic approximation (4.5). The first curve corresponds to $z = 0.2$, and the loss of accuracy of the large-z approximation in the region of the initial peak is evident, with both height and sharpness being overestimated. This trend clearly arises from the increasing dominance of the sharp initial peak of β, shown in figure 4, as z is reduced (since the β contribution is multiplied by z^{-1} in (4.5)). Nevertheless, over the remainder of the range of time, the asymptotic approximation agrees closely with the numerical values. The next two curves, for $z = 0.3$ and 0.4, show successively smaller inaccuracies in the neighbourhood of the initial peak, and the final one, for $z = 0.6$, is virtual indistinguishable from the numerical values.

Finally, figure 7 compares different cross-sectional averages of the concentration, again at $z = 0.3$. These correspond to: area-weighted averaging, flow-weighted averaging, measurement on the axis and measurement at the wall. (As discussed above, these solutions can equally be viewed as the area-weighted average concentrations observed for different initial radial distributions, namely: a uniform distribution over the cross-section, a parabolic distribution, tracer concentrated on the axis and tracer concentrated at the wall.) At this relatively short distance downstream from the point of release, the radial differences in concentration are considerable, except in the immediate neighbourhood of $t = 0.3$. One aspect illustrated by these results is the variation of the mean transit time μ_∞, i.e. the mean value of t associated with the transient. This is smallest for measurement on the axis ($\mu_\infty \approx 0.258$), where the flow velocity has its maximum, and largest for measurement at the wall ($\mu_\infty \approx 0.383$). Similarly the temporal variance σ_∞^2 increases from 0.00608 on the axis to 0.0104 at the wall; as shown by (3.9)–(3.11), the absolute differences in μ_∞ and σ_∞^2 persist even at large distances downstream, where the Gaussian form has developed. Another prominent feature of the undeveloped profiles shown in figure 7 is the variation of the shape of the curve with radial position, particularly regarding the relative sizes of the two peaks. In fact, the second peak is absent on the axis, and there is no suggestion of an initial peak at the wall, where the curve appears far closer to the Gaussian form: in quantitative terms, we find from (3.9) that the coefficient of skewness $\nu_\infty^3/\sigma_\infty^3$ at the wall is only 0.320, compared with 0.911 on the axis.

Note that at the wall the predicted concentration falls below zero for a small period immediately following the onset, because the negative contribution of β outweighs that of α. Although the approximation is uniformly asymptotic for fixed τ as $z \to \infty$,

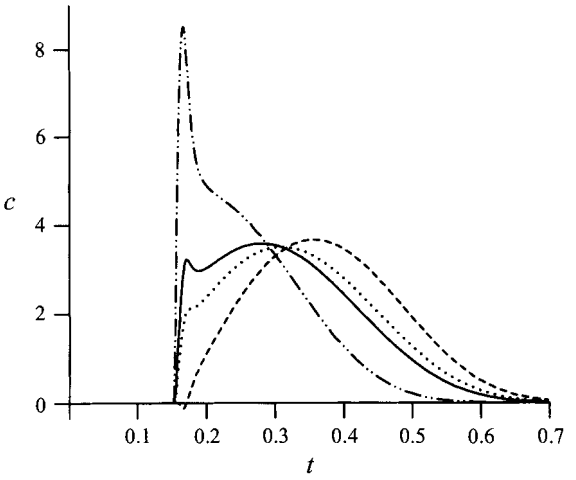

FIGURE 7. Cross-sectional integrals of the concentration as a function of dimensionless time t, at a dimensionless distance $z = 0.3$ downstream of the point of release, assuming a uniform initial distribution over the cross-section. We show integrals corresponding to: $-\cdots-\cdots$, measurement on the axis $r = 0$; ——, a flow-weighted cross-sectional average; $\cdots\cdots$, an area-weighted cross-sectional average; – – – –, measurement at the wall $r = 1$.

as noted in §5.2, for small, fixed values of z the magnitude of α may tend to zero faster than that of β as $\tau \to -\frac{1}{2}$; this does not occur, however, for the flow- or area-weighted averages or at $r = 0$.

6. Application and discussion

The object of this paper is twofold: (i) to consider the development of dispersion in shear flow by calculating characteristics of the temporal concentration variation at a fixed position, rather than by the more usual approach in which the spatial distribution is calculated at a fixed time, and (ii) to derive a uniformly valid asymptotic approximation for the whole of this concentration distribution, including the tails. The adoption of the temporal approach means that the results are more directly applicable to experiments in which measurements are made using a fixed sensor, and are also potentially useful for the treatment of dispersion in systems of tubes arranged sequentially, for example in bifurcating networks, where it is necessary to deduce the time-varying efflux out of each section from knowledge of the time-varying influx at the inlet. In this connection note that, when the Péclet number is infinite, the flow-weighted cross-sectional average of concentration is directly proportional to the total axial flux of tracer: it is therefore easy to express fluxes in terms of the present solution. The expressions derived in this paper are approximations formally valid for large values of the dimensionless axial distance z from the point of discharge, defined by (2.1). In practice, however, they are found to be reasonably accurate even for quite small values of this parameter.

The general solution outlined in §§3 and 4 applies directly to dispersion in a tube of arbitrary cross-section, with an arbitrary axial velocity profile. It is clear that the technique can straightforwardly be extended to include features such as transversely non-uniform diffusivity and exchange between phases. It may also be capable of extension to dispersion in more complicated systems such as spatially periodic media.

6.1. *Application of results for the temporal moments*

The first set of results presented (§3) is for the moments of the time-dependent concentration variation measured at a fixed axial position; these are the temporal counterparts of the axial moments which have been in common use since the work of Aris (1956). For dispersion by an arbitrary flow profile within a tube of arbitrary cross-section, the temporal moments when the Péclet number is finite are given in terms of those for the infinite-Péclet-number case by (3.4). In §3.2 we give temporal moments, when the Péclet number is infinite, for the particular case of Poiseuille flow. In (3.9) the mean, variance and third moment about the mean are given in dimensionless form, in the case where the tracer substance is introduced at a (dimensional) distance ar_0, and measured at a (dimensional) distance ar, from the axis. From these equations may be deduced the moments corresponding to an arbitrary initial radial distribution and an arbitrary radially weighted average of the measured concentration. For the most commonly considered initial condition, that of a radially uniform tracer distribution, the temporal moments for cross-sectional and flow-weighted averages of the measured concentration are given by (3.10) and (3.11) respectively. When the Péclet number is infinite, the latter are equivalent to temporal moments of the total tracer flux passing a fixed axial position.

As an illustration, we show how to recover from these equations the dimensional form of the flow-weighted temporal moments when the Péclet number is finite. The first step is to substitute the infinite-Péclet-number moments, given by (3.11), into (3.4) to obtain their finite-Péclet-number counterparts. These moments are then re-dimensionalized by multiplication by appropriate powers of the timescale a^2/D used for non-dimensionalization in (2.1). Finally, the dimensionless variables P and z are re-expressed in terms of dimensional quantities using (2.1) and (2.2). The resulting equations, for the dimensional mean, variance and third moments about the mean, are

$$M_f = V_m^{-1}Z + DV_m^{-2}(\tfrac{1}{48}P^2 + 2) + \ldots, \tag{6.1a}$$

$$\Sigma_f^2 = DV_m^{-3}(\tfrac{1}{24}P^2 + 2)Z + D^2V_m^{-4}(-\tfrac{23}{11520}P^4 + \tfrac{7}{24}P^2 + 8) + \ldots, \tag{6.1b}$$

$$N_f^3 = D^2V_m^{-5}(\tfrac{1}{320}P^4 + \tfrac{1}{2}P^2 + 12)Z + D^3V_m^{-6}(-\tfrac{1367}{3870720}P^6 + \tfrac{11}{384}P^4 + \tfrac{15}{4}P^2 + 64) + \ldots, \tag{6.1c}$$

in which the error terms omitted are exponentially small in DZ/V_ma^2. Although these results are for a particular initial transverse distribution and weighting of the measured concentration, in fact the terms proportional to Z are independent of both these conditions (as is the final constant term in each case).

The true temporal moments given by (6.1) can be compared with those obtained from a Taylor-type Gaussian approximation (Levenspiel & Smith 1957). The latter are found to give correctly the dominant, Z-dependent terms of the first two moments, but to fail to predict the dominant term of N_f^3, proportional to P^4Z. Although there are also some other terms in common with the true moments, the leading constant terms of the mean and variance are also predicted incorrectly, so that there are relative errors of order V_ma^2/DZ for the first two moments. (Note, however, that if the cross-sectionally averaged, rather than the flow-weighted, moments are considered, the Gaussian approximation does predict M_f correctly.)

6.2. *Application of the asymptotic approximation for tracer concentration*

The principal result presented in this paper is a uniformly asymptotic approximation for the time-dependent tracer concentration measured at a fixed axial position. In §4, for an arbitrary flow profile in a tube of arbitrary cross-section, we calculate a Green's function, corresponding to an initial introduction of tracer at some point in the fluid with transverse (dimensionless) position $\boldsymbol{r}_0$, which describes the measured concentration with the transverse (dimensionless) position $\boldsymbol{r}$. The dimensionless form of this Green's function G_∞, for infinite Péclet number, is given by (4.5). In this equation, z and τ are dimensionless axial and time variables (given in terms of dimensional quantities by (6.4) below). In general, the functions ϕ, α and β, and the parameter κ, must be evaluated by numerical calculation, by following a procedure which can be summarized in four steps as follows. The first stage is to solve the two-dimensional reaction–diffusion-type equation (2.14) over the cross-section of the tube, with a boundary condition of the form (2.5) at the wall, in order to determine the smallest eigenvalue ℓ_0 as a function of the Laplace transform variable s. Secondly, from the corresponding eigenfunction $f_0(\boldsymbol{r};s)$, the function $F_0(\boldsymbol{r}_0,\boldsymbol{r};s)$ is evaluated using (4.3). Thirdly, the location of the saddle point in the s-plane, s_τ, is found by solution of (4.4). Finally, the quantities required for the general solution are found from (4.6) and (4.7), in which they are expressed as combinations of the s-derivatives of ℓ_0 and F_0, evaluated at $s = s_\tau$. The dimensional concentration may then be recovered from (2.1)–(2.3) as

$$C = \frac{\mathscr{M}D}{\pi V_m a^4} G_\infty \left(\frac{\boldsymbol{R}}{a}, \frac{DZ}{V_m a^2}, \frac{DT}{a^2}; \frac{\boldsymbol{R}_0}{a} \right), \tag{6.2}$$

in units of mass per unit volume. From the Green's function, as explained in §4, it is straightforward to deduce the solution for an arbitrary initial transverse distribution and an arbitrary transverse weighting of the measured concentration, by replacing the functions $f_0(\boldsymbol{r}_0;s)$ and $f_0(\boldsymbol{r};s)$ where they appear in (4.3) by appropriate weighted averages.

For Poiseuille flow, the constant κ is equal to $\frac{1}{48}$, and numerical results are presented in §5.4 for ϕ (figure 1) and for several weighted transverse averages of α and β (figures 3 and 4). (In addition, the graphs of $f_0(r;s_\tau)$ in figure 2 show how, at leading order, the concentration varies over the cross-section at different times.) Using these results, as in figures 5–7, it is possible to evaluate the general approximation in its dimensionless form (4.5) for any values of z and t. As illustrated in figures 5 and 6, the general approximation agrees reasonably closely with numerically calculated concentration profiles even for quite small values of z. In particular, it reproduces the double-peaked profile observed at short distances, and so represents a significant improvement on earlier asymptotic approximations. (Significant differences between the asymptotic solution and the numerical results are confined to a fairly small region near the first peak.) Another feature of the solution for small values of z, illustrated in figure 7, is a strong dependence of the concentration on transverse position. This means that there is a need for caution in interpreting measurements when either the initial distribution or the mode of sampling is not well characterized, and in the early stages of development the different transversely weighted averages of concentration will differ significantly. Traditionally, dispersion has been studied in terms of the cross-sectional average of concentration, although this is rather difficult to measure in practice, unless by optical means. We have chosen instead to present results for the flow-weighted average of concentration, which when the Péclet number is infinite

has a direct physical significance, being proportional to the total axial tracer flux. In practical applications, however, for comparison with concentration measurements made using a particular sampling technique, the transverse weighting should reflect the amounts sampled at different transverse positions.

Although the general approximation (4.5) is required to describe the whole concentration distribution, simpler approximations are available for particular ranges of time. In particular, the approximation for the central region, appropriate when $\tau \ll 1$, may be regarded as a refinement of Taylor's Gaussian approximation, and will be adequate for many purposes. This approximation is calculated for Poiseuille flow in §5.1, and may be straightforwardly found for other flow profiles and cross-sectional geometries from small-s series solutions of the type given in §3.2. As an example, we give here the dimensional form of this approximation when the initial tracer distribution is radially uniform and when the measured concentration is averaged using a flow weighting. This case corresponds to the approximations (5.2a) for ϕ and (5.4) for the appropriate averages of α and β. Substituting these into (4.5) and using (6.2), we find

$$\langle vC \rangle = \frac{2\sqrt{3}\mathscr{M}D^{1/2}}{\pi^{3/2}V_m^{1/2}a^3Z^{1/2}}\left(1 - \tfrac{2}{5}\tau + \tfrac{87}{70}\tau^2 - \tfrac{11}{4480}z^{-1} + \ldots\right)\exp\left(-z(12\tau^2 - \tfrac{36}{5}\tau^3 + \tfrac{4197}{350}\tau^4)\right), \tag{6.3}$$

in which, as in general, z and τ are given in terms of dimensional quantities by

$$z = DZ/V_m a^2, \qquad \tau = Z^{-1}(V_m T - Z). \tag{6.4}$$

In (6.3), the terms within the exponent are independent of both the initial tranverse distribution of tracer and the transverse weighting of the measured concentration. The other correction terms may easily be found for other conditions by using (5.2), in which the functions $f_{0j}(r_0)$ and $f_{0j}(r)$ should be replaced by averages, weighted by the initial distribution and the final weighting respectively.

By including in the exponent powers of τ beyond the quadratic, this expression improves Taylor's Gaussian approximation and its subsequent refinements (Chatwin 1970; Stokes & Barton 1990). The latter fail to describe the concentration distribution, even at leading order, beyond $t^{1/6}(\sim z^{1/6})$ standard deviations from the peak, which is the point at which the cubic term in the exponent rises to order unity. Equation (6.3), on the other hand, does not break down until $t^{3/10}(\sim z^{3/10})$ standard deviations from the peak; the range of validity could be extended further by including still higher powers of τ in the exponent.

Another simpler version of the general result is applicable when $\tau \gg 1$, and describes the decay of the concentration at long times. The dimensional forms of the cross-sectional and flow-weighted averages of concentration can be obtained, as described above, by substituting (5.15) and (5.16) respectively into (6.2). We can deduce from this solution the (dimensional) time T_ϵ that elapses before the concentration drops to some very small fraction ϵ of its peak value (in practice ϵ must be $O(\mathrm{e}^{-DZ/V_m a^2})$). At leading order, we find that T_ϵ satisfies

$$\frac{V_m T_\epsilon}{Z} \sim \left[\phi_0^{-1}\frac{V_m a^2}{DZ}\ln(\epsilon^{-1})\right]^{1/3}. \tag{6.5}$$

(This approximation can easily be improved using (5.14)–(5.16), although the corrections depend on the initial transverse distribution and the cross-sectional weighting of the observed concentration.) Note that, since the large-τ solution is determined by behaviour close to the wall, provided that the no-slip condition applies there, the

same scalings (though not the same multiplicative constants) will apply for tubes with different cross-sections and axial flow profiles.

The true asymptotic result (6.5) can be compared with the estimate obtained using Taylor's Gaussian approximation, namely

$$\frac{V_m T_\epsilon}{Z} \sim 4\kappa \frac{V_m a^2}{DZ} \ln(\epsilon^{-1}), \tag{6.6}$$

and that obtained from the temporal Gaussian approximation (4.8), namely

$$\frac{V_m T_\epsilon}{Z} \sim \left[4\kappa \frac{V_m a^2}{DZ} \ln(\epsilon^{-1})\right]^{1/2}. \tag{6.7}$$

In the limit $\epsilon \to 0$, both (6.6) and (6.7) overestimate the time taken for the concentration to fall to this level.

C.G.P. is grateful for support by a Wellcome Trust Research Fellowship, and S.R.K. for support by the Leverhulme Trust. The authors are grateful to Professor A. M. Lenhoff for kindly supplying data from computational solutions (published with A. Shankar) for comparison with the present work. They also thank Dr K. H. Parker for helpful comments on the manuscript.

Appendix A. Results for the axial distribution

A.1. *Moments of the axial distribution*

For comparison with the results for moments of the temporal concentration distribution, we give here the corresponding expressions for axial moments, which will be denoted by a superscript (z). Most of these have appeared before, though they have often been given for particular initial conditions or cross-sectional averages, first by Aris (1956; though note that his equations contain some errors), and later by Chatwin (1970), Gill & Sankarasubramanian (1970) and Smith (1981*b*, 1982*a*, 1984).

It is easy to show that, in contrast to (3.4), the axial moments for finite and infinite P are linked by the simple relationships

$$\mu^{(z)} = \mu_\infty^{(z)}, \qquad \sigma^{(z)2} = \sigma_\infty^{(z)2} + 2P^{-2}t, \qquad \nu^{(z)3} = \nu_\infty^{(z)3}. \tag{A 1}$$

The axial moments may be conveniently calculated by a procedure similar to that in §§2,3, but in which the Laplace transform is inverted first, and the Fourier transform is expressed as a small-k series. We find

$$\mathscr{F} G_\infty(\boldsymbol{r}, k, t; \boldsymbol{r}_0) = \pi \sum_{n=0}^{\infty} \frac{f_n^{(z)}(\boldsymbol{r}_0; k) f_n^{(z)}(\boldsymbol{r}; k)}{\int_K f_n^{(z)}(\boldsymbol{r}'; k)^2 \, \mathrm{d}A'} \exp\left(s_n^{(z)}(k) t\right), \tag{A 2}$$

where the $f_n^{(z)}$ and $s_n^{(z)}$ both depend on k, being eigensolutions and eigenvalues of the equation

$$\nabla_r^2 f_n^{(z)} - \left(s_n^{(z)} + \mathrm{i}kv(\boldsymbol{r})\right) f_n^{(z)} = 0. \tag{A 3}$$

A small-k series solution is found, giving

$$\left.\begin{aligned} s_0^{(z)}(k) &= -\mathrm{i}k - \tfrac{1}{48}k^2 + \tfrac{1}{2880}\mathrm{i}k^3 + O(k^4), \\ f_0^{(z)}(r; k) &= 1 - \mathrm{i}f_{01}^{(z)}(r)k - f_{02}^{(z)}(r)k^2 + \mathrm{i}f_{03}^{(z)}(r)k^3 + O(k^4), \end{aligned}\right\} \tag{A 4}$$

where the functions $f_{0i}^{(z)}(r)$ can be expressed in terms of the $f_{0i}(r)$, defined by (3.8), as

$$f_{01}^{(z)}(r) = f_{01}(r), \quad f_{02}^{(z)}(r) = f_{02}(r) + \tfrac{1}{48} f_{01}(r), \quad f_{03}^{(z)}(r) = f_{03}(r) + \tfrac{1}{24} f_{02}(r) + \tfrac{1}{2880} f_{01}(r). \tag{A 5}$$

Substituting (A 4) into (A 2) and using the relationship between the axial moments and the derivatives of $\mathscr{F}G_\infty$ at $k = 0$ (corresponding to (3.1) for the temporal moments), we find that

$$\mu_\infty^{(z)} = t + \tfrac{1}{6} + f_{01}(r_0) + f_{01}(r) + o(1), \tag{A 6a}$$

$$\sigma_\infty^{(z)2} = \tfrac{1}{24} t - \tfrac{17}{2880} + \left(\tfrac{1}{24} f_{01}(r_0) - f_{01}(r_0)^2 + 2 f_{02}(r_0)\right) + \left(\tfrac{1}{24} f_{01}(r) - f_{01}(r)^2 + 2 f_{02}(r)\right) + o(1), \tag{A 6b}$$

$$\begin{aligned} \nu_\infty^{(z)3} = {} & \tfrac{1}{480} t - \tfrac{83}{75600} \\ & + \left(\tfrac{1}{480} f_{01}(r_0) - \tfrac{1}{8} f_{01}(r_0)^2 + 2 f_{01}(r_0)^3 - 6 f_{01}(r_0) f_{02}(r_0) + \tfrac{1}{4} f_{02}(r_0) + 6 f_{03}(r_0)\right) \\ & + \left(\tfrac{1}{480} f_{01}(r) - \tfrac{1}{8} f_{01}(r)^2 + 2 f_{01}(r)^3 - 6 f_{01}(r) f_{02}(r) + \tfrac{1}{4} f_{02}(r) + 6 f_{03}(r)\right) + o(1) \end{aligned} \tag{A 6c}$$

as $t \to \infty$. When the initial distribution over the cross-section is uniform, the area-weighted cross-sectionally averaged spatial moments, denoted by a subscript a, are

$$\mu_{\infty a}^{(z)} = t, \quad \sigma_{\infty a}^{(z)2} = \tfrac{1}{24} t - \tfrac{1}{360} + o(1), \quad \nu_{\infty a}^{(z)3} = \tfrac{1}{480} t - \tfrac{17}{53760} + o(1) \tag{A 7a–c}$$

and the flow-weighted averaged moments, denoted by a subscript f, are

$$\mu_{\infty f}^{(z)} = t + \tfrac{1}{48} + o(1), \quad \sigma_{\infty f}^{(z)2} = \tfrac{1}{24} t - \tfrac{29}{11520} + o(1), \quad \nu_{\infty f}^{(z)3} = \tfrac{1}{480} t - \tfrac{1691}{3870720} + o(1). \tag{A 8a–c}$$

A.2. *Asymptotic approximation for the axial distribution*

It is easily shown using (4.1) that an equivalent version of (4.5) for the axial distribution is

$$G_\infty(\boldsymbol{r}, z, t; \boldsymbol{r}_0) = \frac{\mathrm{e}^{-t\phi^{(z)}(\zeta)}}{2(\pi\kappa t)^{1/2}} \left(\alpha^{(z)}(\boldsymbol{r}_0, \boldsymbol{r}, \zeta) + t^{-1}\beta^{(z)}(\boldsymbol{r}_0, \boldsymbol{r}, \zeta) + O(t^{-2})\right), \tag{A 9}$$

in the limit $t \to \infty$ with the rescaled axial distance ζ fixed, where

$$\zeta = t^{-1}(z - t), \tag{A 10}$$

and the functions in (A 9) are defined in terms of their temporal counterparts by

$$\phi^{(z)}(\zeta) = (1 + \zeta)\,\phi\left(-(1 + \zeta)^{-1}\zeta\right), \tag{A 11a}$$

$$\alpha^{(z)}(\boldsymbol{r}_0, \boldsymbol{r}, \zeta) = (1 + \zeta)^{-1/2}\,\alpha\left(\boldsymbol{r}_0, \boldsymbol{r}, -(1 + \zeta)^{-1}\zeta\right), \tag{A 11b}$$

$$\beta^{(z)}(\boldsymbol{r}_0, \boldsymbol{r}, \zeta) = (1 + \zeta)^{-3/2}\,\beta\left(\boldsymbol{r}_0, \boldsymbol{r}, -(1 + \zeta)^{-1}\zeta\right). \tag{A 11c}$$

A number of expressions for these functions can be deduced from the results given in the main body of the paper. Here we give the asymptotic approximations valid near the edges of the distribution.

For the 'leading' tail, we find from (5.9) that as $\zeta \to 1$, the area- and flow-weighted average concentrations are given by

$$\langle c\rangle(z, t) \sim \tfrac{1}{2}\langle vc\rangle(z, t) = \frac{2^{3/2}\mathrm{e}^{-t\phi^{(z)}(\zeta)}}{(\pi t)^{1/2}(1 - \zeta)^{1/2}} \left(1 + O((1 - \zeta), t^{-1}(1 - \zeta)^2)\right), \tag{A 12}$$

in which we deduce from (5.5) that

$$\phi^{(z)}(\zeta) = 2(1 - \zeta)^{-1} + o(1). \tag{A 13}$$

For the 'trailing' tail, in the limit $\zeta \to -1$, we find from (5.15) that the (area-weighted) cross-sectional average concentration is

$$\langle c\rangle(z,t) = \frac{Q_1^2 \mathrm{e}^{-t\phi^{(z)}(\zeta)}}{3\lambda_0 Q_0(\pi t)^{1/2}(1+\zeta)}\left(1 + O((1+\zeta), t^{-1}(1+\zeta)^2)\right) \tag{A 14}$$

and from (5.16) that the flow-weighted average concentration is

$$\langle vc\rangle(z,t) = \frac{2^{1/3}Q_1 Q_2 \mathrm{e}^{-t\phi^{(z)}(\zeta)}}{\lambda_0^{1/3} Q_0(\pi t)^{1/2}}\left(1 + O((1+\zeta), t^{-1}(1+\zeta)^2)\right), \tag{A 15}$$

in which from (5.11) we have

$$\phi^{(z)}(\zeta) = \phi_0^{(z)}(1+\zeta)^{-2} + \phi_1^{(z)}(1+\zeta)^{-1} + \phi_2^{(z)} + o(1), \tag{A 16}$$

in which the coefficients are given by

$$\left.\begin{aligned} \phi_0^{(z)} &= \tfrac{64}{27}|a_1'|^3 \approx 2.507, \quad \phi_1^{(z)} = -\tfrac{32}{45}|a_1'|^3 - \tfrac{8}{5} \approx -2.352, \\ \phi_2^{(z)} &= -\tfrac{16}{315}|a_1'|^3 - \tfrac{1}{25} - \tfrac{9}{100}|a_1'|^{-3} \approx -0.1788, \end{aligned}\right\} \tag{A 17}$$

where a_1' is the first (negative) root of Ai'.

Appendix B. Choice of the integration contours $\mathscr{C}_n$

In (4.2), the contours of integration $\mathscr{C}_n$ for inversion of the Laplace transform are required to pass to the right of the singularities of the respective integrands. Numerical investigation of the behaviour, in the upper half-plane $\mathrm{Im}(s) > 0$, of the eigenvalues $\ell_n^{(a)}(s)$ corresponding to axisymmetric solutions of (2.14) for Poiseuille flow shows that $\ell_0^{(a)}(s)$ (which is smaller than all the non-axisymmetric eigenvalues, and so is identical with $\ell_0(s)$ in (4.2)) has a branch point at $s = b_1$, $\ell_1^{(a)}(s)$ has branch points at $s = b_1$ and b_2, $\ell_2^{(a)}(s)$ has branch points at $s = b_2$ and b_3, and so on. Each of these branch points is locally of the square-root type, and b_n links $\ell_{n-1}^{(a)}(s)$ and $\ell_n^{(a)}(s)$. (In general the location of the branch points will depend on the cross-section of the tube and the form of the axial flow profile.) For Poiseuille flow we find numerically that

$$b_1 \approx -3.629 + 14.012\mathrm{i}, \quad b_2 \approx -0.078 + 32.240\mathrm{i}, \quad b_3 \approx 5.841 + 52.146\mathrm{i}. \tag{B 1}$$

Note that the real parts are increasing, so it appears that it will be impossible to choose a common integration contour $\mathscr{C}$ which lies to the right of all the b_n. But such a contour can be chosen for any truncated version of the series, no matter how many terms it contains.

On the real s-axis, $\ell_0(s)$ is by definition the smallest eigenvalue, so that the first term dominates the series solution (2.19). The corresponding exponent has a unique saddle point at $s = s_\tau$ given by (4.4), and it is tempting to try to invert the first term individually by deforming the integration contour so that it passes through s_τ. But this may lie to the left of the branch point at $s = b_1$, which for some values of τ would give rise to a larger contribution than the saddle point. However, if higher terms of the series are added, we can use the structure of the $\ell_n^{(a)}(s)$ in the complex plane to deform the integration contours so as to make it clear that such contributions from the branch points cancel, leaving a dominant contribution from the saddle point.

For illustration, take a version of (4.2) truncated after three terms, and consider a situation in which s_τ lies to the left of the branch points b_n. Choose initially an

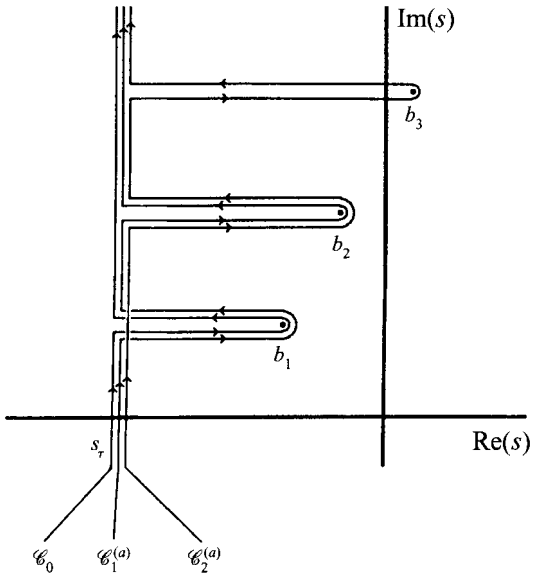

FIGURE 8. Schematic illustration of the choice of integration contours $\mathscr{C}_n^{(a)}$ ($n = 0$, 1 and 2), which are deformed to pass around the branch points b_n ($n = 1$, 2 and 3).

integration contour passing to the right of b_1, b_2 and b_3, and then for each term, deform the contour to the left so as to pass through $s = s_\tau$, leaving excursions around the branch points encountered during deformation. The result is as shown schematically in figure 8, with the contours $\mathscr{C}_0$ and $\mathscr{C}_1^{(a)}$ passing around b_1, the contours $\mathscr{C}_1^{(a)}$ and $\mathscr{C}_2^{(a)}$ passing around b_2, and $\mathscr{C}_2^{(a)}$ alone passing around b_3. Careful consideration shows that the integrands are equal on the segment of $\mathscr{C}_0$ approaching b_1 and the segment of $\mathscr{C}_1^{(a)}$ contour leaving it, so the contributions of these two segments cancel each other. The same is true of the remaining two segments passing around b_1, and of the four segments passing around b_2. Thus, apart from contributions associated with b_3 arising from truncation, the presence of the branch points has no effect on the integral. By including enough terms of the series, the truncation terms can be made asymptotically smaller than the contribution from the neighbourhood of the saddle point, and the solution of §4 follows.

Appendix C. Asymptotic forms of the tails

C.1. *Asymptotic solution for* $\tau \to -\frac{1}{2}$

We require asymptotic approximations for f_0 and ℓ_0 in the limit $s \to \infty$. From (2.14), for Poiseuille flow the governing equation is

$$r^{-1}\frac{\mathrm{d}}{\mathrm{d}r}\left(r\frac{\mathrm{d}f_0}{\mathrm{d}r}\right) - \left(s - 2\ell_0(s)(1-r^2)\right) f_0 = 0. \tag{C 1}$$

This equation, and the condition $f_0(0) = 1$, are satisfied by

$$f_0^{(0)}(r;s) = \exp\left(-\tfrac{1}{2}\gamma_1(s)r^2\right), \tag{C 2a}$$

$$\ell_0^{(0)}(s) = \tfrac{1}{2}s + \gamma_1(s), \tag{C 2b}$$

in which

$$\gamma_1(s) = (s+1)^{1/2} + 1. \tag{C 3}$$

This leaves the condition at $r = 1$ unsatisfied. Examination of (C 1) shows that this condition influences the form of f_0 over the small lengthscale $s^{-1/2}$. Consequently, in a thin layer near the wall the leading-order solution is

$$f_0(r;s) \sim B_1(s)\cosh\left(s^{1/2}(1-r)\right), \tag{C 4}$$

and the condition of matching with (C 2*a*) requires that $B_1(s) \sim 2\mathrm{e}^{-\gamma_1(s)/2}$ (with algebraically smaller errors). The correction to f_0 outside this layer (like that to ℓ_0) is exponentially small.

Substituting from (C 2*b*) into (4.4), we obtain

$$\tfrac{1}{2}(s_\tau + 1)^{-1/2} - \tfrac{1}{2} + o(1) = \tau, \tag{C 5}$$

from which the position of the saddle point is determined as

$$s_\tau = \tfrac{1}{4}(\tau + \tfrac{1}{2})^{-2} - 1 + o(1), \tag{C 6}$$

in which the error term is exponentially small. Evaluating the functions in (C 2) at $s = s_\tau$ leads straightforwardly to (5.6), (5.7) in §5.2, and also to the leading-order approximation for ϕ in (5.5).

The correction function β can be found similarly by using this approximate solution in (4.7*c*). It is found that both the area-weighted cross-sectional average of β and its value at $r = 0$ are exponentially small as $\tau \to -\frac{1}{2}$. However, the flow-weighted average in this limit is given by

$$\langle v\beta \rangle \sim \frac{2(\tau + \frac{1}{2})^{3/2}}{3^{1/2}(\tau+1)^3}. \tag{C 7}$$

The correction term in (5.5) can be obtained by extending the approximate solution (C 2) to one of the form

$$f_0(r;s) = f_0^{(0)}(r;s) + f_0^{(1)}(r;s) + \ldots, \tag{C 8a}$$

$$\ell_0(s) = \tfrac{1}{2}s + \gamma_1(s) + \gamma_2(s) + \ldots \tag{C 8b}$$

The governing equation for $f_0^{(1)}$ is found to be

$$r^{-1}\frac{\mathrm{d}}{\mathrm{d}r}\left(r\frac{\mathrm{d}f_0^{(1)}}{\mathrm{d}r}\right) - \left(s - (s + 2\gamma_1(s))(1-r^2)\right) f_0^{(1)} = -2\gamma_2(s)(1-r^2)f_0^{(0)}, \tag{C 9}$$

subject to boundary conditions

$$f_0^{(1)} = 0 \qquad \text{at } r = 0, \tag{C 10a}$$

$$\frac{\mathrm{d}f_0^{(1)}}{\mathrm{d}r} = -\frac{\mathrm{d}f_0^{(0)}}{\mathrm{d}r} = \gamma_1(s)\mathrm{e}^{-\gamma_1(s)/2} \qquad \text{at } r = 1. \tag{C 10b}$$

Also, from (C 4),

$$f_0^{(1)} \sim f_0^{(0)} = \mathrm{e}^{-\frac{1}{2}\gamma_1(s)} \qquad \text{at } r = 1, \tag{C 11}$$

with algebraically smaller errors. Applying Green's theorem to the functions $f_0^{(0)}$ and $f_0^{(1)}$, and using the governing equations (C 1) and (C 9) together with (C 2*a*), we find that

$$\gamma_2(s) \sim -\frac{2\gamma_1(s)^3}{\gamma_1(s) - 1}\mathrm{e}^{-\gamma_1(s)}, \tag{C 12}$$

again with algebraically smaller errors. The improved approximation (5.5) for $\phi(\tau)$ follows from this result after a little more manipulation.

C.2. *Asymptotic solution for* $\tau \to \infty$

We require asymptotic approximations for f_0 and ℓ_0 in the limit $s \to -\infty$. In this case we expect f_0 will be largest in a thin region near the wall $r = 1$, and exponentially smaller elsewhere. A balance can be achieved between the terms of (C 1) by means of the scalings

$$y = (-s)^{1/2}(1-r), \qquad \ell_0 \sim -\lambda_0(-s)^{3/2}; \tag{C 13}$$

the resulting form of the equation is

$$\frac{\mathrm{d}^2 f_0}{\mathrm{d}y^2} = (4\lambda_0 y - 1)f_0 + \ldots, \tag{C 14}$$

in which the size of terms omitted relative to those retained is $(-s)^{-1/2}$. This suggests a series development for ℓ_0 of the form

$$\ell_0(s) = -\lambda_0(-s)^{3/2} - \lambda_1(-s) - \lambda_2(-s)^{1/2} - \lambda_3 + O(-s)^{-1/2}, \tag{C 15}$$

with a similar series for f_0, except that since f_0 is constrained to be of order unity near the axis, it will be exponentially large in s near the wall, and its size must be determined by matching with the solution in the interior. Matching requires that $f_0 \to 0$ as $y \to \infty$, and together with the condition of zero gradient at the wall, this defines an eigenvalue problem which determines λ_0. The smallest eigenvalue corresponds to, at leading order,

$$f_0(r;s) \sim B_2(s)\mathrm{Ai}\left((4\lambda_0)^{1/3}y - (4\lambda_0)^{-2/3}\right), \qquad \text{with } \lambda_0 = \tfrac{1}{4}|a_1'|^{-3/2} \approx 0.2431, \tag{C 16}$$

in which a_1' is the first (negative) root of Ai$'$, and $B_2(s)$ must be determined by matching with the solution in the interior. By a straightforward but tedious regular perturbation calculation the higher-order corrections can be found in terms of Airy functions and their derivatives, and application of the boundary condition at $r = 1$ allows the constants λ_1, λ_2 and λ_3 to be determined. In this way we find that

$$\left.\begin{aligned} \lambda_1 &= \tfrac{1}{10} + \tfrac{9}{40}|a_1'|^{-3} \approx 0.3128, \\ \lambda_2 &= \tfrac{8}{175}|a_1'|^{3/2} + \tfrac{27}{200}|a_1'|^{-3/2} + \tfrac{27}{160}|a_1'|^{-9/2} \approx 0.3335, \\ \lambda_3 &= \tfrac{64}{2625}|a_1'|^{3} + \tfrac{431}{2625} + \tfrac{27}{500}|a_1'|^{-3} + \tfrac{27}{250}|a_1'|^{-6} \approx 0.3376. \end{aligned}\right\} \tag{C 17}$$

Substituting the resulting series solution for ℓ_0 into (4.4), solving for s_τ and using the definition (4.7*a*), we obtain a series approximation for ϕ as $\tau \to \infty$, of the form (5.11), with coefficients given by

$$\left.\begin{aligned} \phi_0 &= \tfrac{64}{27}|a_1'|^3 \approx 2.507, \quad \phi_1 = \tfrac{32}{5}|a_1'|^3 - \tfrac{8}{5} \approx 5.168, \\ \phi_2 &= \tfrac{592}{105}|a_1'|^3 - \tfrac{81}{25} - \tfrac{9}{100}|a_1'|^{-3} \approx 2.637, \\ \phi_3 &= \tfrac{4184}{2625}|a_1'|^3 - \tfrac{9223}{5250} - \tfrac{27}{500}|a_1'|^{-3} - \tfrac{27}{800}|a_1'|^{-6} \approx -0.1525. \end{aligned}\right\} \tag{C 18}$$

To determine $B_2(s)$ in (C 16), it is necessary to find an asymptotic approximation for f_0 in the region away from the wall. Application of the WKBJ method gives, for the range with $r \gg (-s)^{-3/4}$ and $1 - r \gg (-s)^{-1/2}$,

$$f_0(r;s) \sim B_3(s) r^{-1/2}(1-r^2)^{-1/4} \exp\left(\int_0^r \left(s - 2\ell_0(s)(1-r'^2)\right)^{1/2} \mathrm{d}r'\right). \tag{C 19}$$

Using (5.10) the exponent is found to be equal to

$$2^{-1/2}\lambda_0^{1/2}\left(r(1-r^2)^{1/2}+\sin^{-1}r\right)(-s)^{3/4}$$
$$+2^{-3/2}\lambda_0^{-1/2}\left(\lambda_1 r(1-r^2)^{1/2}-(1-\lambda_1)\sin^{-1}r\right)(-s)^{1/4}+o(1)\quad \text{as } s\to-\infty. \tag{C 20}$$

Finally, the solution (C 19) is found to break down when r becomes comparable with $(-s)^{-3/4}$, and in this range we find instead

$$f_0(r;s)\sim I_0\left(2^{1/2}\lambda_0^{1/2}(-s)^{3/4}r\right), \tag{C 21}$$

in which the condition $f_0=1$ at $r=0$ has been used to determine the multiplicative constant. Now matching with (C 19), (C 20) determines $B_3(s)$, and further matching with (C 16) gives $B_2(s)$. Finally, evaluating these solutions for f_0 in the three regions at $s=s_\tau$ (and of course retaining all but the asymptotically small contributions to the exponent of (C 19)) gives (5.12).

The dominant contributions to the cross-sectional integrals of f_0 come from the thin region near the wall where the function is exponentially large. For use in (4.3), the integral $\int v f_0^2\,\mathrm{d}A$ is required, and to leading order it can be expressed in terms of the integral

$$Q_0=\int_{a_1'}^{\infty}(u-a_1')\mathrm{Ai}(u)^2\,\mathrm{d}u\approx 0.1985, \tag{C 22}$$

while the cross-sectional averages occurring in (5.15), (5.16) are expressed in terms of

$$Q_1=\int_{a_1'}^{\infty}\mathrm{Ai}(u)\,\mathrm{d}u\approx 0.8091, \tag{C 23a}$$

$$Q_2=\int_{a_1'}^{\infty}(u-a_1')\mathrm{Ai}(u)\,\mathrm{d}u\approx 0.8243. \tag{C 23b}$$

REFERENCES

Aris, R. 1956 On the dispersion of a solute in a fluid flowing through a tube. *Proc. R. Soc. Lond.* A **235**, 67–77.

Camacho, J. 1993 Purely global model for Taylor dispersion. *Phys. Rev.* E **48**, 310–321.

Chatwin, P. C. 1970 The approach to normality of the concentration distribution of a solute in a solvent flowing along a straight pipe. *J. Fluid Mech.* **43**, 321–352.

Chatwin, P. C. 1980 Presentation of longitudinal dispersion data. *J. Hydraul. Div. ASCE* **106**, 71–83.

Gill, W. N. & Sankarasubramanian, R. 1970 Exact analysis of unsteady convective diffusion. *Proc. R. Soc. Lond.* A **316**, 341–350.

Gill, W. N. & Sankarasubramanian, R. 1971 Dispersion of a non-uniform slug in time-dependent flow. *Proc. R. Soc. Lond.* A **322**, 101–117.

Levenspiel, O. & Smith, W. K. 1957 Notes on the diffusion-type model for the longitudinal mixing of fluids in flow. *Chem. Engng Sci.* **6**, 227–233.

Lighthill, M. J. 1966 Initial development of diffusion in Poiseuille flow. *J. Inst. Maths Applics.* **2**, 97–108.

Shankar, A. & Lenhoff, A. M. 1989 Dispersion in laminar flow in short tubes. *AIChE J.* **35**, 2048–2052.

Shankar, A. & Lenhoff, A. M. 1991 Dispersion in round tubes and its implications for extra-column dispersion. *J. Chromatogr.* **556**, 235–248.

Smith, R. 1981*a* A delay-diffusion description for contaminant dispersion. *J. Fluid Mech.* **105**, 469–486.

Smith, R. 1981*b* The importance of discharge siting upon contaminant dispersion in narrow rivers and estuaries. *J. Fluid Mech.* **108**, 43–53.

SMITH, R. 1982*a* Gaussian approximation for contaminant dispersion. *Q. J. Mech. Appl. Maths* **35**, 345–366.

SMITH, R. 1982*b* Non-uniform discharges of contaminants in shear flows. *J. Fluid Mech.* **120**, 71–89.

SMITH, R. 1984 Temporal moments at large distances downstream of contaminant releases in rivers. *J. Fluid Mech.* **140**, 153–174.

SMITH, R. 1985 Contaminant dispersion as viewed from a fixed position. *J. Fluid Mech.* **152**, 217–233.

SMITH, R. 1987*a* Diffusion in shear flows made easy: the Taylor limit. *J. Fluid Mech.* **175**, 201–214.

SMITH, R. 1987*b* Shear dispersion looked at from a new angle. *J. Fluid Mech.* **182**, 447–466.

SMITH, R. 1990 An easy-to-use formula for contaminant dispersion. *J. Fluid Mech.* **215**, 195–207.

SMITH, R. 1995 Multi-mode models of flow and of solute dispersion in shallow water. Part 1. General derivation. *J. Fluid Mech.* **283**, 231–248.

STOKES, A. N. & BARTON, N. G. 1990 The concentration distribution produced by shear dispersion of solute in Poiseuille flow. *J. Fluid Mech.* **210**, 201–221.

TAYLOR, G. I. 1953 Dispersion of soluble matter in solvent flowing slowly through a tube. *Proc. R. Soc. Lond.* A **219**, 186–203.

TAYLOR, G. I. 1954 Conditions under which dispersion of a solute in a stream of solvent can be used to measure molecular diffusion. *Proc. R. Soc. Lond.* A **225**, 473–477.

TSAI, Y. H. & HOLLEY, E. R. 1978 Temporal moments for longitudinal dispersion. *J. Hydraul. Div. ASCE* **104**, 1617–1634.

TSAI, Y. H. & HOLLEY, E. R. 1980 Temporal moments for longitudinal dispersion. *J. Hydraul. Div. ASCE* **106**, 2063–2066.

ULTMAN, J. S. & WEAVER, D. W. 1979 Concentration sampling methods in relation to the computation of a dispersion coefficient. *Chem. Engng Sci.* **34**, 1172–1174.

YOUNG, W. R. & JONES, S. 1991 Shear dispersion. *Phys. Fluids* A **3**, 1087–1101.